

Modeling sea level changes and geodetic variations by glacial isostasy: the improved SELEN code

Giorgio Spada

Dipartimento di Scienze di Base e Fondamenti (DiSBeF)

Università di Urbino “Carlo Bo”

Urbino, Italy

`giorgio.spada@gmail.com`

Daniele Melini

Istituto Nazionale di Geofisica e Vulcanologia (INGV)

Roma, Italy

Gaia Galassi

Dipartimento di Scienze di Base e Fondamenti (DiSBeF)

Università di Urbino “Carlo Bo”

Urbino, Italy

Florence Colleoni

Centro Euro-Mediterraneo sui Cambiamenti Climatici (CMCC)

Bologna, Italy

November 27, 2024

Abstract

We describe the basic features of SELEN, an open source Fortran 90 program for the numerical solution of the so-called “Sea Level Equation” for a spherical, layered, non-rotating Earth with Maxwell viscoelastic rheology. The Sea Level Equation was introduced in the 70s to model the sea level variations in response to the melting of late-Pleistocene ice-sheets, but it can be also employed for predictions of geodetic quantities such as vertical and horizontal surface displacements and gravity variations on a global and a regional scale. SELEN (acronym of SEa Level EquatioN solver) is particularly oriented to scientists at their first approach to the glacial isostatic adjustment problem and, according to our experience, it can be successfully used in teaching. The current release (2.9) considerably improves the previous versions of the code in terms of computational efficiency, portability and versatility. In this paper we describe the essentials of the theory behind the Sea Level Equation, the purposes of SELEN and its implementation, and we provide practical guidelines for the use of the program. Various examples showing how SELEN can be configured to solve geodynamical problems involving past and present sea level changes and current geodetic variations are also presented and discussed.

Keywords: Sea Level Equation – Glacial Isostatic Adjustment – Relative Sea Level – Geodetic Variations

1 Introduction

The physical processes governing sea level changes of glacio-isostatic and hydro-isostatic origin have been thoroughly studied in the last decades. They are described in the so-called “Sea Level Equation” (hence after referred to as SLE), the integral equation first introduced

by Farrell and Clark (1976) to model sea level variations following the melting of late-Pleistocene ice-sheets. The SLE is also currently employed to study the sea level changes associated with present terrestrial ice melting in response to global warming (e.g. Mitrovica et al. 2001), a critical issue for its potential impact on environment and society (Solomon et al., 2007). The variation of currently observed geodetic quantities (3-D crustal deformations, gravity variations, altimetric and tide gauges signals) are directly affected by the melting of past and present ice sheets. However, they are also sensitive to the meltwater component of the surface load, whose time evolution is governed by the same equation. The wide spectrum of possible applications of the SLE confirms the central role of glacial isostatic adjustment (GIA) in the framework of both satellite (Peltier, 2004) and ground-based geodetic investigations (King et al., 2010).

SELEN is an open source program written in Fortran 90, primarily designed to simulate the sea level and geodetic variations in response to the melting of continental ice sheets. SELEN provides a numerical solution to the SLE and gives access to various related quantities of interest for geodynamics and geodesy. The program, which was first introduced in a primitive form by Spada and Stocchi (2007) and now obsolete (hereafter referred to as SELEN 1.0), has recently been deeply re-organized and improved in a number of aspects, ranging from the structure of the program to the computational performance and portability. In particular, all components have been reviewed and optimized, and various utilities have been added to facilitate the numerical solution to problems of geodetic relevance, as the time-variations of the harmonic coefficients of the gravity field. Recently, SELEN 2.9 has been successfully employed, for practical applications in the context of GIA, within the 2nd Training School on Glacial Isostatic Adjustment Modeling, held in Gävle (Sweden) in June 2011. The feedback from the students and from a number of scientists involved in various fields of geodynamics and geodesy, who are routinely working with SELEN, have greatly contributed to improve the code previously released by Spada and Stocchi (2007) and has stimulated the release of this upgraded version.

Though the principal physical ingredients of the SLE are implemented in SELEN, some approximations are adopted. First, SELEN assumes a linear incompressible rheology and a spherically symmetric undeformed Earth. Therefore, the program takes advantage from the viscoelastic Green’s function formalism (see Peltier 1974 and references in Spada et al. 2011). Consequently, lateral rheological variations are not taken into account. As a second approximation, possible effects of the Earth’s rotational fluctuations upon sea level variations are not modeled. As discussed by Milne and Mitrovica (1998), the rotational effects are important in some particular regions of the globe, but not large enough to invalidate the whole solution of the SLE. Third, following Farrell and Clark (1976), SELEN does not account for the horizontal migration of shorelines in response to sea level change. This indeed constitutes a crude approximation especially in areas of shallow bathymetry, which will be relaxed in the future releases of SELEN so to allow for “gravitationally self-consistent” paleogeographical reconstructions (Peltier, 2004). Finally, it is important to remark that SELEN does not account for tectonic contributions to sea level, for local effects such as subsidence driven by sediment loading, nor any possible anthropic contribution to sea level change. Furthermore, SELEN does not account for ocean dynamics or possible steric sealevel variations, nor it accounts for ice dynamics. The challenging topic of the coupling between the SLE, the ocean circulation and the continental cryosphere is left to others.

This manuscript is not self-contained. An exhaustive description of the technical details is avoided here, and emphasis is given on the general features of SELEN and the discussion of a set of case studies of general relevance. The theory behind SELEN has been illustrated in detail by Spada and Stocchi (2006, 2007), to which the reader is also referred for references to the most important papers published on this topic. SELEN does *not* come with an user guide. However, the comments across all Fortran program units and the self-explanatory SELEN configuration file should be sufficient. The paper is organized as follows. The physics behind SELEN is briefly summarized in Section 2. Section 3 illustrates how SELEN works. Section 4 introduces a few case studies where SELEN is employed to model past sea level variations (subsection 4.1) and present-day variations of geodetic quantities (4.2). Finally, in Section 5 we draw our conclusions.

SELEN is free software and anyone is welcome to distribute it under certain conditions within the terms of a Global Public License (GPL) (for details, visit <http://www.gnu.org/licenses/>). The

SELEN package is available upon request to the authors.

2 Theory

Here we briefly illustrate the background theory of the SLE, the integral equation that describes the sea level variations and solid Earth deformations associated with GIA. Essentially, the material that follows is a condensed summary of the SLE theory first exposed by Farrell and Clark (1976), on which SELEN is based. In addition, some theory notes will also be provided in Section 4 to discuss specific SELEN outputs. For further details, including the numerical implementation of the so-called “pseudo-spectral” method (Mitrovica and Peltier, 1991; Mitrovica et al., 1994) on which SELEN relies upon, the reader is referred to the review of Spada and Stocchi (2006) and to references therein.

As it will appear from the synthesis below, the SLE (and its numerical implementation) does not involve absolute quantities and can, consequently, only provide *variations* of geophysical and geodetic quantities relative to a reference state. To clearly illustrate what SELEN is actually computing, it is convenient to first define “sea level” as

$$\text{SL}(\omega, t) = R_{ss} - R_{se}, \quad (1)$$

where $\omega \equiv (\theta, \lambda)$, θ is colatitude and λ is longitude, t is time, and with R_{ss} and R_{se} we denote the radius of the (equipotential) sea surface and of the solid surface of the Earth, both relative to the Earth’s center of mass, respectively. Quantity $\text{SL}(\omega, t)$, which has indeed an “absolute” character, is *not* what SELEN is solving for. Rather, the quantity involved in the SLE is sea level *change*

$$S(\omega, t) = \text{SL}(\omega, t) - \text{SL}(\omega, t_r), \quad (2)$$

where t_r is a reference time that, in the numerical applications of the SLE generally denotes a remote epoch prior to the beginning of ice melting. Hence, from (1), the definition of sea level change suitable for GIA studies is

$$S(\omega, t) = N - U, \quad (3)$$

where N represents the sea surface *variation* and U is the vertical displacement of the solid surface of the Earth. Basically, Eq. (3) represents the SLE in its simplest form; what follows is aimed to illustrate the relationship between S and the variations of the ice thickness through time, in order to obtain a form amenable to a numerical approach.

According to Farrell and Clark (1976), N can be written as

$$N(\omega, t) = G + c, \quad (4)$$

where c is a yet undetermined function of time, and the geoid height variation is

$$G(\omega, t) = \frac{\Phi}{\gamma}, \quad (5)$$

in which γ is the reference gravity at the surface of the Earth and $\Phi(\omega, t)$ is the total variation of the gravity potential. Hence, using Eq. (5) into (3) gives

$$S(\omega, t) = \frac{\Phi}{\gamma} - U + c, \quad (6)$$

where mass conservation of the system (Ice sheets + Oceans) is ensured taking

$$c = -\frac{m_i(t)}{\rho_w A_o} - \overline{\left(\frac{\Phi}{\gamma} - U\right)}, \quad (7)$$

where the density of water ρ_w is assumed to be constant, m_i is the mass variation of the ice sheets, A_o is the (constant) area of the present-day oceans and the overbar indicates the average over the surface of the oceans

$$\overline{(\dots)} = \frac{1}{A_o} \int_o (\dots) dA, \quad (8)$$

where $dA = a^2 \sin \theta d\theta d\lambda$ is the area element and a is Earth average radius. From Eq. (6), the SLE can be therefore written as

$$S(\omega, t) = \left(\frac{\Phi}{\gamma} - U \right) + S^E - \overline{\left(\frac{\Phi}{\gamma} - U \right)}, \quad (9)$$

where the “eustatic” sea level variation

$$S^E(t) = -\frac{m_i}{\rho_w A_o}, \quad (10)$$

shows the remarkable property $S^E = \overline{S^E}$. The SLE has solution $S = S^E$ only in the case of a rigid, non self-gravitating Earth ($U = \Phi = 0$ in Eq. 9).

Functions $U(\omega, t)$ and $\Phi(\omega, t)$ will depend on the spatiotemporal variations of the surface load. This is expressed by

$$\mathcal{L}(\omega, t) = \rho_i I + \rho_w S \mathcal{O}, \quad (11)$$

where the two terms on the right hand side are associated with the waxing and waning of the ice sheets, and with the redistribution of meltwater in the ocean basins, respectively. In Eq. (11), ρ_i is ice density, \mathcal{O} is the “ocean function” ($\mathcal{O} = 1$ on the oceans, and $\mathcal{O} = 0$ on land), and

$$I(\omega, t) = T - T_0, \quad (12)$$

is the ice thickness variation, where $T(\omega, t)$ is absolute ice thickness, and $T_0(\omega)$ is a reference thickness (e.g. the thickness at the Last Glacial Maximum, LGM, 21 kyrs ago). The mass variation in Eq. (10) is obtained from (12) by integration over the ice-covered regions:

$$m_i(t) = \int_i \rho_i I dA. \quad (13)$$

According to Eq. (11), vertical displacement stems from two terms

$$U(\omega, t) = \rho_i G_u \otimes_i I + \rho_w G_u \otimes_o S, \quad (14)$$

where G_u is the Green’s function for vertical displacements, \otimes_i and \otimes_o are spatio-temporal convolutions over the ice- and ocean-covered regions, respectively. Similarly

$$\Phi(\omega, t) = \rho_i G_\phi \otimes_i I + \rho_w G_\phi \otimes_o S, \quad (15)$$

where G_ϕ is the Green’s function for incremental gravitational potential. Explicit expressions for G_u and G_ϕ are given in Spada and Stocchi (2006) in terms of the load-deformation coefficients (LDCs) $h(t)$ and $k(t)$, respectively. Introducing the sea level Green’s function G_s as

$$\frac{G_s}{\gamma}(\omega, t) = \frac{G_\phi}{\gamma} - G_u, \quad (16)$$

substitution of Eqs. (15) and (14) into (9) gives

$$S(\theta, \lambda, t) = \frac{\rho_i}{\gamma} G_s \otimes_i I + \frac{\rho_w}{\gamma} G_s \otimes_o S + S^E - \frac{\rho_i}{\gamma} \overline{G_s \otimes_i I} - \frac{\rho_w}{\gamma} \overline{G_s \otimes_o S}, \quad (17)$$

which represents the SLE in the “gravitationally self-consistent” form that is numerically implemented in SELEN. Since the unknown $S(\omega, t)$ also appears in the spatiotemporal convolutions at the right-hand side, the SLE is an integral equation, which cannot be solved explicitly unless some drastic simplifying assumptions are made (Spada and Stocchi, 2006). The SLE is a linear equation as long as shorelines are not allowed to migrate horizontally, i.e. if \mathcal{O} (and consequently A_o) are not time-dependent. Sea level variations are sensitive to mantle rheology through G_s , since this is determined by the viscoelastic LDCs h and k (Spada, 2003; Spada and Stocchi, 2006). Solutions of Eq. (17) in special cases, discussed in detail by Spada and Stocchi (2006), are also available via SELEN.

3 How SELEN works

Running SELEN requires a standard UNIX (including Linux and Mac OS X) environment and a Fortran 90 compiler. On Windows systems, SELEN can run within the Cygwin environment, freely downloadable from <http://www.cygwin.com>. A list of supported operating systems and Fortran compilers is given in the (simple text) configuration file `config.dat`. While the previous version of SELEN (1.0) was limited to the IBM XL commercial compiler, SELEN 2.9 components can be compiled both using the freely available g95 (<http://www.g95.org>) and gfortran (<http://gcc.gnu.org/gfortran>) compilers, or the commercial Intel Fortran compiler. Additional configurations for the operating system and compilers in SELEN 2.9 can be implemented by modifying the setup program `config.f90`. To run SELEN, the GMT (Generic Mapping Tools) public domain software of Wessel and Smith (1998) must be installed on the system. In SELEN 2.9, the most computationally intensive portions of code have been parallelized with OpenMP (2005) directives. The corresponding program units can therefore take advantage of multi-threading on modern CPUs, resulting in a substantial performance improvement.

SELEN consists of several (independent) Fortran 90 program units, performing specific computation steps. A list, with a short description of their purpose, is provided in Table 5. The user can specify run parameters in the configuration file `config.dat`; this file is parsed by the setup program `config.f90`, which checks parameters for consistency and creates a shell script (`selen.sh`) containing the compilation and execution commands for the SELEN components needed for the specific run. The configuration and execution process is transparent to the user and entirely handled by the `makeselen.sh` shell script. To launch a SELEN run, the user only needs to edit the `config.dat` file and execute the `makeselen.sh` script. This constitutes a significant improvement with respect to previous version SELEN 1.0, which lacked a flexible user interface. After each run, SELEN outputs are stored in subfolders of the output folder named `depot-name`, created in the working directory, where `name` is a 4-character label defined by the user in the `config.dat` file.

In this way, outputs of different SELEN runs can be stored in the working directory. The structure of the output folder is described in Table 5; a copy of the `config.dat` file is also stored in the output folder for reference.

A typical SELEN run can be subdivided in three main steps: *i*) pre-computing of all the needed functions, *ii*) numerical solution of the SLE and *iii*) computation of geophysical and geodetic quantities requested by the user.

During the first phase, SELEN performs the spherical harmonic (SH) expansions of the ocean function \mathcal{O} and of the ice thickness variation I , and obtains the LDCs h , l and k for the selected Earth model (an Earth model is defined by its elastic and rheological layering according to the conventions adopted for the TABOO program, see Spada 2003). For the numerical evaluation of surface integrals of Eq. (9), SELEN defines an icosahedron-shaped pixelization of the sphere, displayed in Fig. 1. The grid density is controlled by the resolution parameter R , defined in the `config.dat` file; the number of grid pixels is given by $N_p = 40R(R + 1) + 12$. As discussed by Tegmark (1996), an accurate numerical integration is only ensured for $\ell_{max} \leq \sqrt{3N_p}$, where ℓ_{max} is the maximum harmonic degree of the SH expansion. A discrete realization of the ocean function is practically obtained by selecting the grid pixels falling in “wet” and “dry” areas with the `gmtselect` utility from the GMT package (see Fig. 1). To optimize computations involving SH functions, all the needed associated Legendre functions and trigonometric functions at grid pixels are pre-computed once and stored on disk for later re-use. This SH database can be re-used also across different runs, as long as parameters R and ℓ_{max} are unchanged (values of R and ℓ_{max} are defined in the `config.dat` file). Similarly, the SH expansion of the ice load, a relatively time-consuming task, can be re-used by setting the appropriate option in the configuration file `config.dat`.

In the second phase, SELEN solves numerically the SLE. As discussed in Section 2, the SLE is an integral (implicit) equation, in which the unknown S is convolved in space and time with the sea level Green’s functions. An iterative solution scheme is therefore needed, similar to the one employed in the solution of one-dimensional inhomogeneous integral Fredholm equation of the second kind. As a zero-order solution, SELEN approximates the unknown function S with the

T5

T5

F1

eustatic sea level variation: $S^{(0)} = S^E$. By substituting $S^{(0)}$ in the right-hand side of Eq. (17), a new estimate $S^{(1)}$ is obtained. This process can be iterated any number of times, by using Eq. (17) to obtain the k -th order solution $S^{(k)}$ from the $(k-1)$ -th order solution $S^{(k-1)}$, until a pre-determined convergence threshold is reached (i.e. until the ratio $|S^{(k)} - S^{(k-1)}|/|S^{(k)}|$ becomes sufficiently small at all the grid pixels and time steps). According to the numerical tests carried out by Spada and Stocchi (2007) and to our experience, three iterations normally suffice for convergence.

In the third and final phase, SELEN uses the solution of the SLE in the spectral domain to obtain predictions of geophysical and geodetic quantities by SH synthesis. According to the settings in the user configuration file `config.dat`, SELEN can compute present-day rates of deformation (in vertical and horizontal directions), geoid change and sea level change on global or regional scales, relative sealevel predictions at specific sites, sea level change rates at tide gauge stations, present-day velocities at user-specified sites, and present-day rates of variation of the Stokes coefficients of the Earth’s gravity field.

The execution time of SELEN scales with spatial and harmonic resolutions as $t_{exe} \sim N_p N_h$, where N_p is the number of grid pixels and $N_h = (\ell_{max} + 1)(\ell_{max} + 2)/2$ is the number of SH functions with harmonic degree $\ell \leq \ell_{max}$; as a rough approximation, $t_{exe} \sim R^2 \ell_{max}^2$, where R is the resolution parameter. The memory footprint of SELEN follows a similar scaling law. For high resolution runs (large values of ℓ_{max} and consequently of R), disk I/O can become a considerable fraction of t_{exe} , and these relations may no longer be valid. On multi-core systems, SELEN can use multi-threading to reduce computation time (multi-threading was not implemented in previous version SELEN 1.0). To enable multi-threading, the corresponding option in `config.dat` must be set, specifying the number of threads that SELEN will create. The number of threads should be equal to the number of cores in the system; it can be smaller if the user wishes to leave some resources free for other tasks.

4 A few case studies

To illustrate the main features of SELEN, we have configured the program for a GIA simulation based on model ICE-5G (Peltier, 2004). In the previous version (SELEN 1.0) this ice model, which is now widely employed in the GIA literature, was not accessible. The configuration file `config.dat` for this run (referred to as TEST run) and all the SELEN output files (text files and plots) are available in the folder `depot-TEST` that comes with the SELEN distribution package. The numerical results presented below are organized into two subsections. In the first (Section 4.1), the focus is on the Relative Sea Level (RSL) variations driven by GIA since the LGM, 21 kyrs ago. The second (Section 4.2) is about the delayed viscoelastic effects that GIA is still producing today, and the focus is on the time variations of various geodetic quantities. Keeping separate the two time scales helps to simplify the presentation of the results. However, it should be kept in mind that the present-day geodetic variations depend on the whole history of deglaciation, and are thus extremely sensitive to mantle viscosity in spite of the long time elapsed since the end of melting of major continental ice sheets (e.g. Peltier 2004).

The viscosity profile employed in the cases studies illustrated below is a three-layer volume-average of the original, multi-layered “VM2” profile introduced by Peltier (2004) and associated with the ICE-5G model. Values of viscosity and other parameters that define the incompressible Earth model (hereafter referred as to VM2a) are summarized in Table 5. The isostatic relaxation spectrum determined by SELEN for VM2a is shown in Fig. 2, while Fig. 3 shows the elastic and fluid LDCs. SELEN incorporates TABOO (Spada, 2003; Spada et al., 2004) as a subroutine for computing these spectra, based on the Viscoelastic Normal Modes theory (Peltier, 1974). After execution, all the information about the LDCs (tables with ASCII data and plots, if requested) are made available to the user in folder `depot-TEST/Love-Numbers-by-TABOO`, including the viscous parts of the LDCs (not shown here). All the ensuing SELEN results are obtained using LDCs in the range of degrees $1 \leq \ell_{max} \leq 128$ and are expressed in the reference frame with origin the Earth center of mass (hence, differently than in SELEN 1.0, here we properly account for the

T5
F2
F3

degree $\ell = 1$ LDCs). LDCs of harmonic degree $\ell = 0$ vanish identically because of incompressibility, but they would not play any role even for an compressible Earth since the SLE includes explicitly the constraint of mass conservation (see Eq. 7). The SLE is solved iteratively on the grid shown in Fig. 1 and three iterations are performed to ensure convergence of the iteration scheme (Spada and Stocchi, 2007).

The spatial distribution of the ice thickness according to model ICE-5G at the LGM and at present time are shown in the SELEN plots of Fig. 4. The ICE-5G thickness data are obtained from the home page of Prof. W. R. Peltier (the version with 1° resolution is used). In folder **ICE-MODELS** of the main SELEN directory, other ice models are available, including the previous ICE-X models developed by Prof. W. R. Peltier and co-workers (SELEN also incorporates individual components of the global ICE-5G model, which could be useful for regional studies). Using specific Fortran formats described in program **config.f90**, the user can indeed introduce other *ad hoc* ice models according to specific purposes. In the specific case of ICE-5G, the spatiotemporal discretization has been slightly modified for the sake of computational convenience (details on the discretization scheme adopted in SELEN are available in Spada and Stocchi 2007). The original ICE-5G time grid has been converted into a uniformly spaced 1-kyr grid, and the elementary “rectangular” $1^\circ \times 1^\circ$ ice elements that define ICE-5G are converted, at run time, into equal-area and equal-thickness “discs” that allow for a straightforward SH decomposition because of their symmetry (see e.g. Spada and Stocchi 2006). Since in SELEN 2.9 fixed shorelines are assumed, the melting of the ice distributed across the continental shelf in Fig. 4 (top) is not accompanied by a transgression of ocean water, which may imply a local error in sea level change predictions (this restriction will be relaxed in future releases of SELEN). The equivalent sea level (ESL), shown in Fig. 5, provides the time-history of the ice volume of ICE-5G since the LGM. After execution, all the ice model data are stored in **depot-TEST/ICE5G**. These include the spatial distribution of the ice masses at all times, the ESL function, the SH coefficients of the ice thickness and the SH reconstruction of the ice distribution (options for these computations are available in file **config.dat**).

F4

F5

4.1 Past Relative Sea Level variations

One of the purposes of SELEN is the modeling of sea level variations that occurred during the time period elapsed since the LGM, in consequence of the melting of late-Pleistocene ice sheets. There is a considerable amount of literature about this problem, and it is impossible to provide an exhaustive summary in this paper. A flavor of the enormous importance that past sea level variations have on our understanding of present-day variations is given by e.g. Lambeck and Chappell (2001) and Peltier (2004) and references therein.

In this section, we provide an illustration of the SELEN outputs regarding “Relative Sea Level” (RSL). This quantity is not directly obtained from the SLE (17), which provides $S(\omega, t)$. According to the geological practice, RSL is defined as the difference between SL at a given epoch before present ($t = t_{BP}$) and the present-time ($t = t_p$) value:

$$\text{RSL}(\omega, t_{BP}) = \text{SL}(\omega, t_{BP}) - \text{SL}(\omega, t_p), \quad (18)$$

which, using the definition of sea level given by Eq. (1), can be also written as

$$\text{RSL}(\omega, t_{BP}) = S(\omega, t_{BP}) - S(\omega, t_p), \quad (19)$$

showing that RSL can indeed be obtained from the solution of the SLE computed at two different times (we note that RSL does not depend on the choice of the remote time t_r in Eq. (2)). All the following RSL computations have been obtained performing three iterations within the solution scheme of the SLE, which generally provides a sufficiently accurate solution (see the test computations in Spada and Stocchi 2007).

SELEN can be easily configured for producing RSL predictions at sites of interest to the user, for which observations of past sea levels can be obtained from the literature. Fig. 6, produced by SELEN, shows the locations of 392 sites for which radiocarbon-controlled RSL data are available,

F6

according to the compilation of Tushingham and Peltier (1992, 1993). Information on the sites coordinates and RSL observations, including their uncertainties, are contained in file `sealevel.dat`, obtained from the National Oceanic and Atmospheric Administration (NOOA) page ¹. The RSL observations in this file cover the last 15,000 years and are obtained from various sources, mainly based on geomorphologic and archaeological methods. In the scatterplot of Fig. 7, all RSL observations from the input file `sealevel.dat` (top frame) are qualitatively compared with predictions obtained from SELEN using the settings in `config.dat` (bottom). The scatterplot gives a clear view of the temporal distribution of the RSL observations from this data collection, which are mainly relative to the last $\sim 8,000$ years. The similarity of the two scatterplots in this figure clearly indicates that the ICE-5G model, in its SELEN implementation, broadly reproduces the RSL observations globally available. Of course, local misfits are possible, as we will discuss below for specific sites. A more rigorous global misfit analysis is also possible using SELEN, oriented to users interested to tackle an optimization problem in which the best fitting model parameters (i.e. the viscosity of mantle layers) are to be inverted from a specific set of RSL observations (the results of the misfit analysis for this run, not reproduced here, are available in the folder `depot-TEST/rsl/rsl-misfit`).

F7

Fig. 8 shows a RSL analysis, in which SELEN is programmed to produce RSL predictions at individual sites. Here we only show eight curves out of the 392 available in folder `depot-TEST/rsl/rsl-curves` after the execution of SELEN, all relative to the case of the Hudson Bay. The process of GIA across the Hudson Bay has been the subject of various investigations in the past, because of the sensitivity shown by the uplift data on the rheological layering of the mantle (Mitrovica and Peltier, 1992; Cianetti et al., 2002). RSL observations from this region, shown by error bars in Fig. 8, clearly indicate a monotonous sea level fall that is typical of sites belonging to previously ice-covered areas during the LGM. Model predictions reproduce the RSL observations very satisfactorily. This should not come as a surprise, since the two basic components of model ICE-5G (namely, the chronology of the late-Pleistocene ice sheets and the viscosity profile of the mantle) have been expressly designed to best fit a global dataset of RSL observations, which includes these Hudson bay sites (Peltier, 2004). The further example of Fig. 9 shows results for eight RSL sites in the far field of the previously ice-covered regions, where the history of sea level rise has been less influenced by the direct effect of ice melting. The shapes of the RSL curves in these regions clearly depart from those of the Hudson bay in Fig. 8. In some cases, they neatly indicate a monotonous sea level rise, but some remarkable exceptions are found, in which they show sea level high-stands or more complex features. Their trend is reasonably reproduced by our SELEN computations.

F8

F9

In Fig. 10 we show the results of further runs, in which the program has been configured to solve the SLE using various approximations. The ice model and the rheology are the same as in previous computations. This kind of analysis, which is performed here only for the sites of Richmond (Hudson bay) and of Merseyside (England), is not meant to test the agreement of RSL predictions with observations. Rather, it can be useful to illustrate the role played by some of the basic physical ingredients of the SLE. The solid curves still show the “gravitationally self-consistent” (GSC) solution, in which the SLE is solved in the full form given by Eq. (17). In results shown by dotted RSL curves, only the elastic (EL) components of the LDCs are employed in the computations, hence neglecting the viscous components of the Maxwell rheology. The eustatic curve (EU, dashed), shows the RSL trend obtained assuming a rigid Earth and neglecting any gravitational interaction between the solid Earth, the ice masses, and the oceans. The eustatic RSL curve, which is simply expressed by Eq. 10, is the same for all RSL sites. Finally, the dash-dotted curve (W) shows the solution of the SLE in the so-called “Woodward approximation” (see Spada and Stocchi 2007), in which the Earth is assumed to be perfectly rigid (LDCs are $h = l = k = 0$), and only the gravitational attraction between the ice masses and the oceans is taken into account. From the results of Fig. 10, it is apparent that the RSL observations across the Hudson bay, where ice melting has produced a huge uplift, can only be explained invoking the “gravitationally self-consistent” solution. However, in the case of the far-field site Merseyside, the

F10

¹See http://www1.ncdc.noaa.gov/pub/data/paleo/paleocean/relative_sea_level/.

GSC solution can be assimilated to any of the approximate solutions (including those pertaining to a rigid Earth, EU and W), at least for the last few kiloyears.

The site-by-site analyses shown in Figs 9 and 10 above are useful for a detailed reconstruction of the local RSL curves and direct comparison with observations. However, a global or regional visualization of the RSL variations can be more useful for a qualitative interpretation. For the purpose of visualization of the relative sea level variations associated with GIA, SELEN can be configured in two different ways. Both features were not directly accessible to the user in SELEN 1.0. The first, which is oriented to global analyses, allows for the visualization of the so-called “Clark zones” (Clark et al., 1978), i.e. the regions of the globe in which the RSL curves shows similar patterns after the LGM. Numerical results and plots for this analysis, which are not reported here for space limitations, will be accessible for the **TEST** run in folder **depot-TEST/rs1/rs1-zones/** after execution of SELEN. An example of the second possible RSL analysis, which is more oriented to regional investigations, is shown in Fig. 11, where RSL contour plots across the Mediterranean region for times 2, 6 and 10 kyrs BP are drawn. This area is the subject of considerable interest in view of the significant amount of sea level indicators available (Lambeck et al., 2004; Lambeck and Purcell, 2005). Fig. 11 provides a clear regional characterization of the process of sea level rise in the area. Although the RSL pattern shows a considerable complexity, it is apparent that the largest RSL excursions are predicted in the bulk of the basin, in consequence of the broad subsidence caused by the effects of meltwater load (Stocchi and Spada, 2007). Data and maps for this kind of analysis are found in folder **depot-TEST/rs1-contours/**.

F11

4.2 Effects of GIA on present-day geodetic variations

Three-dimensional movements of the solid Earth and gravity variations are still affected significantly by the isostatic disequilibrium in response to the melting of late-Pleistocene ice sheets (see e.g. King et al. 2010). Therefore, it is sometimes necessary to evaluate quantitatively the amplitude of the GIA effects at present time, possibly in order to decontaminate geodetic quantities observed locally or globally. Since for loads of the size of major late-Pleistocene ice sheets the Maxwell relaxation time of the mantle is of the order of a few kilo-years (see e.g. Schubert et al. 2004), the rates of sea level change or other quantities associated with GIA can be effectively considered as constant through a decade to century time scale. Hereinafter, we will consider a few examples in which the SLE is solved for trends of GIA-related quantities. Since solving the SLE implies a temporal discretization of all variables involved (see Spada and Stocchi 2007 for details), in SELEN geodetic trends at a specific place ω are evaluated numerically as

$$\dot{Q} \equiv \frac{dQ}{dt}(\omega, t_p) \approx \frac{Q(\omega, t_p) - Q(\omega, t_p - \Delta)}{\Delta}, \quad (20)$$

where $\Delta = 1$ kyrs is the natural time step in SELEN, and Q here represents any of the fundamental geodetic quantities S (relative sea level variation), U (vertical displacement) and N (sea surface variation) that appear in Eq. 3. Of course, more accurate methods can be implemented by the user for the numerical evaluation of trends. Though here we focus in the effects of melting of past ice sheets on present-day geodetic variations, with minor modifications SELEN can be also employed for the study of the fingerprints (Mitrovica et al., 2001; Tamisiea et al., 2001) of the current terrestrial ice melting. Examples have been recently given by Sørensen et al. (2011) and Spada et al. (2012) for the case study of the melting of the Greenland ice sheet.

Present-day trends \dot{S} , \dot{U} and \dot{N} , computed by means of Eq. (20), are shown in Figs 12, 13 and 14, respectively, for our **TEST** run. Of course, these global maps are not independent of one another, since from the SLE (see Eq. 3), we have e. g. $\dot{N} = \dot{S} + \dot{U}$. To emphasize the regional variations of these GIA signals, the color tables span the range of ± 1 mm/yr. The very complex pattern of sea level change \dot{S} in Fig. 12 is the consequence of the delayed visco-elastic deformations of the solid surface of the Earth, of gravitational interactions between the solid Earth, the ice masses and the oceans, and of the complex shape of continents. For a rigid, non gravitating Earth we would observe $\dot{S} = 0$ everywhere on this map. The \dot{S} pattern in Fig. 12 has been discussed in a number of studies (see e.g. Mitrovica and Milne 2002). Some features are easily interpreted, such as the

F12

F13

F14

broad areas of sea level fall across the formerly glaciated regions and the surrounding sea level rise corresponding to the collapsing forebulges. Some other features, such as the equatorial region of sea level fall, have a more difficult interpretation in terms of ocean siphoning (Mitrovica and Milne, 2002).

The vertical velocity (\dot{U}) map in Fig. 13 clearly shows a strong anti-correlation with \dot{S} , and in particular it very neatly shows that, in the far field of previously glaciated areas, the continents are currently moving up relative to the Earth’s center of mass at rates as large as 0.5 mm/yr. This is ultimately the consequence of the differential movements induced by meltwater loading acting on the oceans floor. Compared with \dot{S} and \dot{U} , the rate of sea surface variation \dot{N} in Fig. 14 is characterized by a smoother pattern globally, which manifests a relatively large energy content of low-degree harmonics. As seen from the Earth’s center of mass, the sea surface is collapsing everywhere at rates between 0 and 0.5 mm/yr, except in the formerly glaciated regions, where we observe an uplift that broadly follows the uplift of the solid surface of the Earth in Fig. 13, but with a significantly smaller amplitude.

In addition to global maps of trends \dot{S} , \dot{U} and \dot{N} , SELEN can similarly produce regional analyses, which were not directly accessible in previous release. An example is shown in Fig. 15 for the Mediterranean region. This figure shows very clearly how GIA is acting across this relatively small, mid-latitude basin: the region is subsiding ($\dot{U} < 0$, middle frame), and though the sea surface is collapsing relative to the Earth’s center of mass ($\dot{N} < 0$, bottom), in the bulk of the Mediterranean relative sea level is rising ($\dot{S} > 0$, top). As discussed in e. g. Stocchi and Spada (2009), meltwater loading, described by the second term on the right hand side of Eq. (11), is the major cause of subsidence. This is indicated by the shape of the contour lines of \dot{U} , which are broadly following the coastlines.

Tide gauge (TG) records hold a central role in all the assessments of the secular global mean sea level rise so far published (see Douglas 1997, Spada and Galassi 2012 and references therein). Since TGs measure the offset between sea surface and the solid Earth, they constitute the experimental realization of the SLE in its basic form, given by Eq. (3). Perhaps it is not fully appreciated by the climate change community that the current estimates of a global sea level rise of 1.8 ± 0.1 mm/yr since 1880 (Douglas, 1997), recently revised to 1.5 ± 0.1 mm/yr by Spada and Galassi (2012), tightly depend on GIA modeling (hence, to a large extent, on the rheology of the solid Earth). In fact, GIA models consistent with RSL observations since the LGM are commonly employed to decontaminate TG trends obtained from long records, in order to fully highlight the effect of secular climate variations on sea level rise (see e. g. Peltier 2001).

Within SELEN, the GIA component of sea level change at TGs is evaluated by

$$r_k^{gia} = \dot{S}(\omega_k, t_p), \quad (21)$$

where t_p is present time, the time derivative of sea level change is given by Eq. (20) and $\omega_k = (\theta_k, \lambda_k)$ denote colatitude and longitude of the k -th TG. Since the Maxwell relaxation time of the bulk of the mantle is of the order of a few kilo-years (see e.g. Schubert et al. 2004), the rate (21) can be effectively considered as constant through the period of the instrumental TG record. In SELEN, a simple analysis can be performed in which predictions of r_k^{gia} are computed at the TG locations. In the **TEST** run of SELEN, we consider the input data collected in file **DATA/rlr-trends.txt**, pertaining to the 1123 Revised Local Reference (RLR) TG stations listed by the Permanent Service for the Mean Sea Level (PSMSL) as of January 22, 2007 (SELEN maps for these data are shown in Fig. 16). Of course, the user can input other data sets, not necessarily containing TG information. Sample outputs of this SELEN analysis are shown in Tables 5 and 5. The first shows results for TGs with records of at least 100 years of RLR observations, while the second shows a selection of Mediterranean TGs with at least 30 years of observations. The two tables are showing GIA predictions for the rate of sea level change r_k^{gia} , but also for the other fundamental geodetic quantities \dot{U} and \dot{N} (a new feature with respect to SELEN 1.0). All data and plots produced by SELEN for the TG analyses illustrated above are found in folder **depot-TEST/tgauges**.

As a final example of a possible geodetic application available within SELEN, we consider the

time-variations of the gravity potential harmonic coefficients. This analysis can be useful, for example, to evaluate the effects of GIA on the gravity variations observed by the NASA/DLR Gravity Recovery and Climate Experiment (GRACE) satellites (see the overview of Tapley et al. 2009). According to SELEN conventions, the GIA-induced total variation of the gravity field potential, evaluated at the Earth’s surface is:

$$\Phi(a, \omega) = \frac{\Gamma M_e}{a} \sum_{\ell=2}^{\ell_{max}} \sum_{m=-\ell}^{\ell} \Phi_{\ell m} \mathcal{Y}_{\ell m}(\omega), \quad (22)$$

where Γ is Newton’s constant, M_e and a are the mass and the average radius of the Earth, ℓ_{max} is the maximum harmonic degree of the analysis (for run **TEST**, $\ell_{max} = 128$), $\Phi_{\ell m}$ are the gravity coefficients in complex form (these obey $\Phi_{\ell-m} = \Phi_{\ell m}^*$) and $\mathcal{Y}_{\ell m}(\omega)$ are the complex 4π -normalized SH functions of harmonic degree ℓ and order m :

$$\mathcal{Y}_{\ell m}(\omega) = \sqrt{(2\ell+1) \frac{(\ell-m)!}{(\ell+m)!}} P_{\ell m}(\cos \theta) e^{im\lambda}, \quad (23)$$

where $P_{\ell m}(\cos \theta)$ are the associated Legendre functions. Note that in Eq. (22), terms of harmonic degree $\ell = 0$ are not included since the total mass of the Earth is conserved, and those of degree $\ell = 1$ vanish since the origin of the reference frames is assumed to coincide with the Earth’s center of mass. It is sometimes more convenient to transform Eq. (22) into an equivalent expansion involving real coefficients. For instance, according to the conventions usually adopted in gravimetry (including GRACE), we can equivalently write

$$\Phi(a, \omega) = \frac{\Gamma M_e}{a} \sum_{\ell=2}^{\ell_{max}} \sum_{m=0}^{\ell} (\bar{c}_{\ell m} \cos m\lambda + \bar{s}_{\ell m} \sin m\lambda) \bar{P}_{\ell m}(\cos \theta), \quad (24)$$

where $\bar{P}_{\ell m}(\cos \theta)$ denotes the “fully normalized” associated Legendre functions, *not* including the Condon–Shortley phase $(-1)^m$. After some straightforward algebra, for the variations of the Stokes coefficients one obtains $(\bar{c}_{\ell m}, \bar{s}_{\ell m}) = (-1)^m \sqrt{2 - \delta_{0m}} \Phi_{\ell m}^*$. Program **stokes.f90** provides, degree-by-degree, the time derivatives $\dot{\bar{c}}_{\ell m}$ and $\dot{\bar{s}}_{\ell m}$, which can be directly compared with trends obtained from monthly GRACE observations (derivatives are numerically evaluated following Eq. 20) in order to assess the GIA effects. Fig. 17 shows the result obtained for run **TEST**, for harmonics up to degree $\ell_{max} = 9$. A similar analysis has been performed recently by Sørensen (2010), using various global ice models from the literature (and available in the ice models directory **ICE-MODELS** of SELEN).

F17

5 Conclusions

We have described the basic features and the essential theory background of SELEN, an open source Fortran 90 program that solves numerically the SLE. Version 2.9, which constitutes a significant improvement of previous version SELEN 1.0, has been developed to respond to the requests of colleagues working on various aspects of GIA, who did not have access to a SLE solver, and for teaching purposes. SELEN, which is the numerical implementation of the SLE theory presented by Farrell and Clark (1976), can be used to efficiently simulate the spatiotemporal variations of several geophysical and geodetic quantities involved in the GIA process. These include relaxation spectra and LDCs computed using user-supplied rheological profiles, the spatial distribution of the continental ice sheets according to several built-in GIA models, predictions of relative sea level variations at specific sites from which observations are available since the LGM, global and regional maps of present-day rates of variations of GIA-induced sea level change and displacements, local predictions for geodetic variations (including vertical and horizontal movements), and time-variations of harmonic coefficients of the gravity field in response to GIA. Refined implementations of SELEN 1.0 have been recently employed in various geodetic contexts, ranging

from the interpretation of GPS data on a regional scale in Greenland (Nielsen et al., 2012), to the correction of GRACE observations aimed at estimating the mass variation in the Mediterranean and in the Black Sea (Fenoglio-Marc et al., 2012), and to the study of the effects of GIA in West Antarctica (Groh et al., 2012) and Greenland (Ewert et al., 2012; Spada et al., 2012).

SELEN is written in standard Fortran 90 and takes advantage of an OpenMP multi-threaded parallelism. It can be installed and compiled on Mac OS, Linux and Windows platforms. Starting from the examples illustrated in this manuscript, the users can customize SELEN in order to solve *ad-hoc* GIA problems or to include new functionalities within the code. According to our experience with the students of the 2nd Training School on Glacial Isostatic Adjustment (GIA) Modeling, where SELEN has been employed for a tutorial introduction to the physics and the phenomenology of GIA, the program may constitute a valuable instrument for scientists at their first approach to this problem. New features such the simulation of the horizontal migration of shorelines in response to sea level change and the realization of the feedback between sea level variations and rotational fluctuations, are under way and will be available with the upcoming version of SELEN (v. 3.0).

Acknowledgments

We thank all the students and the participants to 2nd Training School on Glacial Isostatic Adjustment Modeling, held in Gävle (Sweden) in June 2011, and all the SELEN users for the numerous feedbacks that have contributed to improve the program. Valentina Barletta is acknowledged for providing benchmark test computations and for advice. All computations involving spherical harmonic functions are performed using routines from the **SHTOOLS** package by Mark Wieczorek (see <http://www.ipgp.fr/wieczor/SHTOOLS/SHTOOLS.html>). We thank Max Tegmark for making available the Fortran code for the icosahedral pixelization of the celestial sphere, which is now incorporated in SELEN. All the figures have been drawn using the GMT public domain software (Wessel and Smith, 1998). SELEN is available upon request to the authors. The numerical computations have been partly performed thanks to a CINECA award under the ISCRA (Italian SuperComputing Resource Allocation) initiative, for the availability of high performance computing resources and support through the Class C Projects contract n. HP10CS9J50. This work has been supported by COST Action ES0701 “Improved Constraints on Models of Glacial Isostatic Adjustment”.

<code>config.dat</code>	SELEN configuration file
<code>makeselen.sh</code>	Bash script that executes SELEN
<u>SELEN Input data:</u>	
<code>wdir/DATA</code>	Various input data for RSL analyses and more
<code>wdir/ICE-MODELS</code>	Ice models data
<code>wdir/VSC</code>	Collection of viscosity profiles
<u>Fortran 90 units:</u>	
<code>config.f90</code>	Interpreter of the configuration file
<code>esl.f90</code>	Equivalent Sea Level
<code>geo.f90</code>	Time variations of geodetic quantities
<code>gmaps.f90</code>	Synthesis of geodetic quantities on global maps
<code>harmonics.f90</code>	Include file with Various SH tools and utilities
<code>ms.f90</code>	GMT multi-segment files from ice data
<code>of_dv.f90</code>	Degree variance of the Ocean Function
<code>px.f90</code>	Pixelization tools (including the Tegmark algorithm)
<code>px_rec.f90</code>	Reorganizes the pixelization data
<code>rec_ice.f90</code>	SH reconstruction of the ice thickness
<code>rec_of.f90</code>	SH reconstruction of the Ocean Function
<code>rmaps.f90</code>	Synthesis of geodetic quantities on regional maps
<code>rsl.f90</code>	Relative Sea Level curves
<code>rsl_zones.f90</code>	Geometry of the Relative Sea Level “Clark’s zones”
<code>rslc.f90</code>	Relative Sealevel Contour lines for regional analyses
<code>sh.f90</code>	SHs at the grid pixels
<code>sh_of.f90</code>	SH coefficients for the Ocean Function
<code>sh_rsl.f90</code>	SHs at the RSL sites
<code>sh_rslc.f90</code>	SHs for regional analysis and RSL contours
<code>sh_tgauges.f90</code>	SHs at the TG sites
<code>shape_factors.f90</code>	“Shape factors” for the ice elements
<code>shice.f90</code>	SH decomposition of the ice model
<code>shtools.f90</code>	An SHTOOLS interface for the SH analysis
<code>sle.f90</code>	The SLE solver
<code>stokes.f90</code>	Variations of the Stokes coefficients of the gravity field
<code>tgauges.f90</code>	Present-day rate of sea level change at the TG sites
<code>tb.f90</code>	The TABOO code
<code>wnw.f90</code>	Numerical test for the SH orthogonality

Table 1: Some of the files contained in the SELEN package. Here `wdir` indicates the working directory of SELEN.

Folder:	content:
ICE5G	Data about the ice model
ICE5G/esl	ESL
ICE5G/original	Ice thickness data
ICE5G/reconstructed	SH reconstruction of ice thickness data
ICE5G/sh	SH coefficients of the ice model
Love-Numbers-by-TAB00	Love numbers data
TAB00	TABOO input files
bin	An empty folder
geod	Predictions at geodetic sites
geod/3dmaps	Regional maps (in progress)
geod/sites	Geodetic predictions at specific sites
gmaps	Global geodetic rates (data and plots)
log	Log files of SELEN and TABOO (with summary of Earth parameters)
of	Ocean function data and plots
of/degree_variance	Ocean function degree variance
px	Various pixelization data and plots
rmaps	Regional geodetic rates (data and maps)
rmaps/Antarctica	rates for Antarctica
...	...
rmaps/NorthAmerica	rates for North America
rsl	Relative Sea Level (RSL) data folder
rsl-contours	RSL contour plot
rsl-curves	RSL curves at specific sites
rsl-misfit	Misfit between RSL data and predictions
rsl-scplot	Scatterplot of RSL data
rsl-sites	Data and plots regarding RSL sites
rsl-table	Summary table of RSL data and predictions
rsl-zones	RSL zones
stokes	Stokes coefficients data
tgauges	Tide gauges (TGs)
tgauges-predictions	Predictions at TGs
tgauges-scplots	TG data scatterplot
tgauges-sites	Maps of TG sites
wnw	“Window test” for the ocean function

Table 2: Organization of the SELEN outputs in directory `depot-TEST`. SELEN outputs consist of various plain text, postscript, and pdf files.



RES= 44, N= 75692


 2011 Dec 20 08:55:34 SELEN 2.9

Figure 1: Pixelization of the sphere following the icosahedron-based method proposed by Tegmark (1996) for astrophysical applications, implemented in SELEN. This geometrical tool provides a natural set of Gauss points on the sphere and allows for a straightforward computation of integrals involving SH functions. The number of pixels in the grid is $N_p = 40R(R+1) + 12$, where R is the resolution parameter. Here $R = 44$ (the corresponding grid spacing is ≈ 45 km). The constraint $N_p \geq \ell_{max}^2/3$, which ensures an optimal integration on the sphere (Tegmark, 1996) is largely met (in the TEST run, $\ell_{max} = 128$). Data about the grid, including spherical coordinates of “wet” (oceanic, blue) and “dry” (continental, green) pixels and postscript figures are found in folder `depot-TEST/px`. In SELEN, wet pixels are separated by dry pixels using the GMT program `gmtselect` (Wessel and Smith, 1998). By default, SELEN employs the full resolution coastlines of GMT (`-Df`), and dry (wet) pixels are selected using option `-Ns/k/s/k/s` (`-Nk/s/k/s/k`) of `gmtselect`.

Layer	Radius (km)	Density (kg m ⁻³)	Shear modulus ($\times 10^{11}$ Pa)	Viscosity ($\times 10^{21}$ Pa s)	Gravity (m s ⁻²)
Lithosphere	6281–6371	4120	0.73	∞	9.707
Shallow upper mantle	5951–6281	4120	0.95	0.5	9.672
Transition zone	5701–5951	4220	1.10	0.5	9.571
Lower mantle	3480–5701	4508	2.00	2.7	9.505
Core	0–3480	10925	0.00	0	10.622

Table 3: Model parameters for model VM2a, employed for the `TEST` run of `SELEN`. The whole library of models available within `SELEN` is accessible in the Fortran unit `tb.F90`.

Earth model: NV=3 CODE=2
*Viscosity profile: /2.7 0.5 0.5/*1E21 Pa.s*

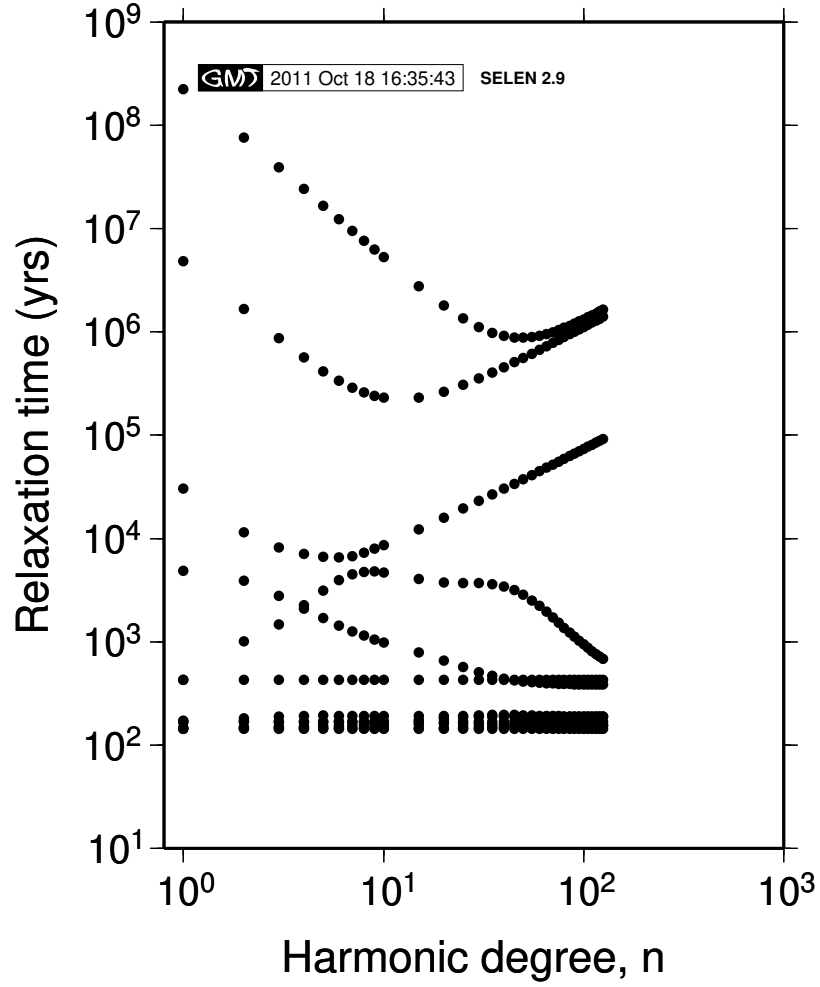
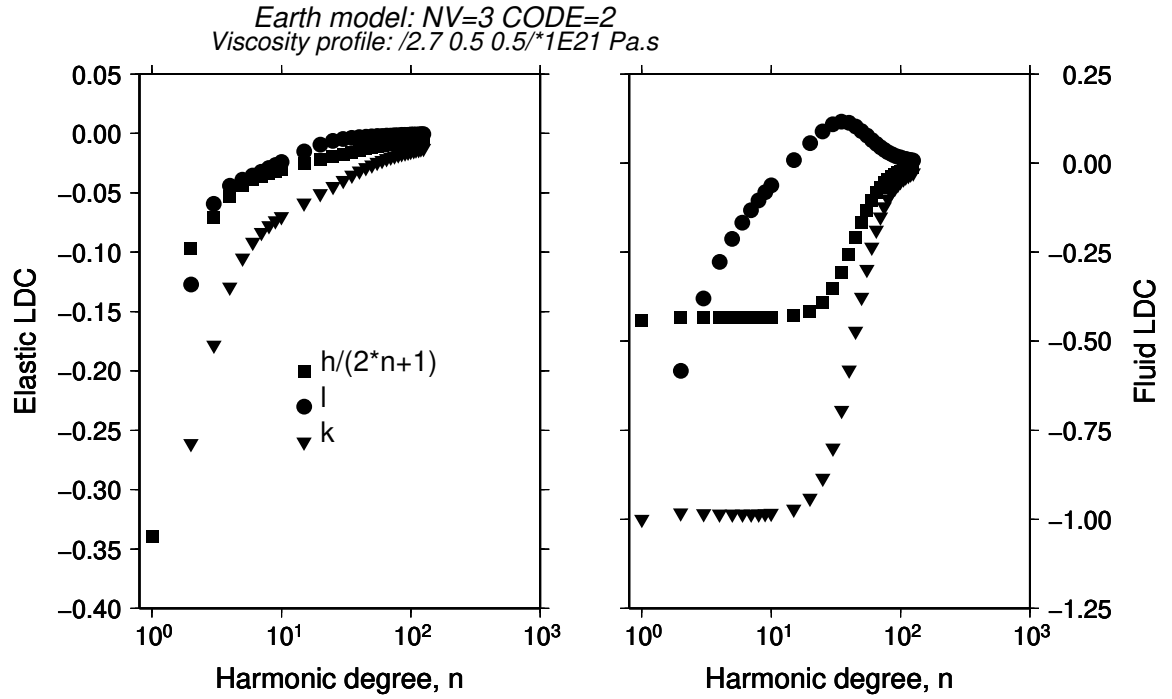


Figure 2: Isostatic relaxation spectrum for model VM2a (see Table 5), showing the relaxation times as a function of harmonic degree $\ell = n$ in the range $1 \leq \ell \leq 128$. The physical meaning of the spectrum is discussed by Spada (2003).



GM 2011 Oct 18 16:35:43 SELEN 2.9

Figure 3: Elastic (left) and fluid (right) values of the LDCs h (associated to vertical displacement), l (horizontal displacement) and k (incremental gravitational potential) for model VM2a (see Table 5), as a function of harmonic degree ℓ . Note that h is normalized by $(2\ell + 1)$. For the definition of the LDCs see e.g. Spada (2003).

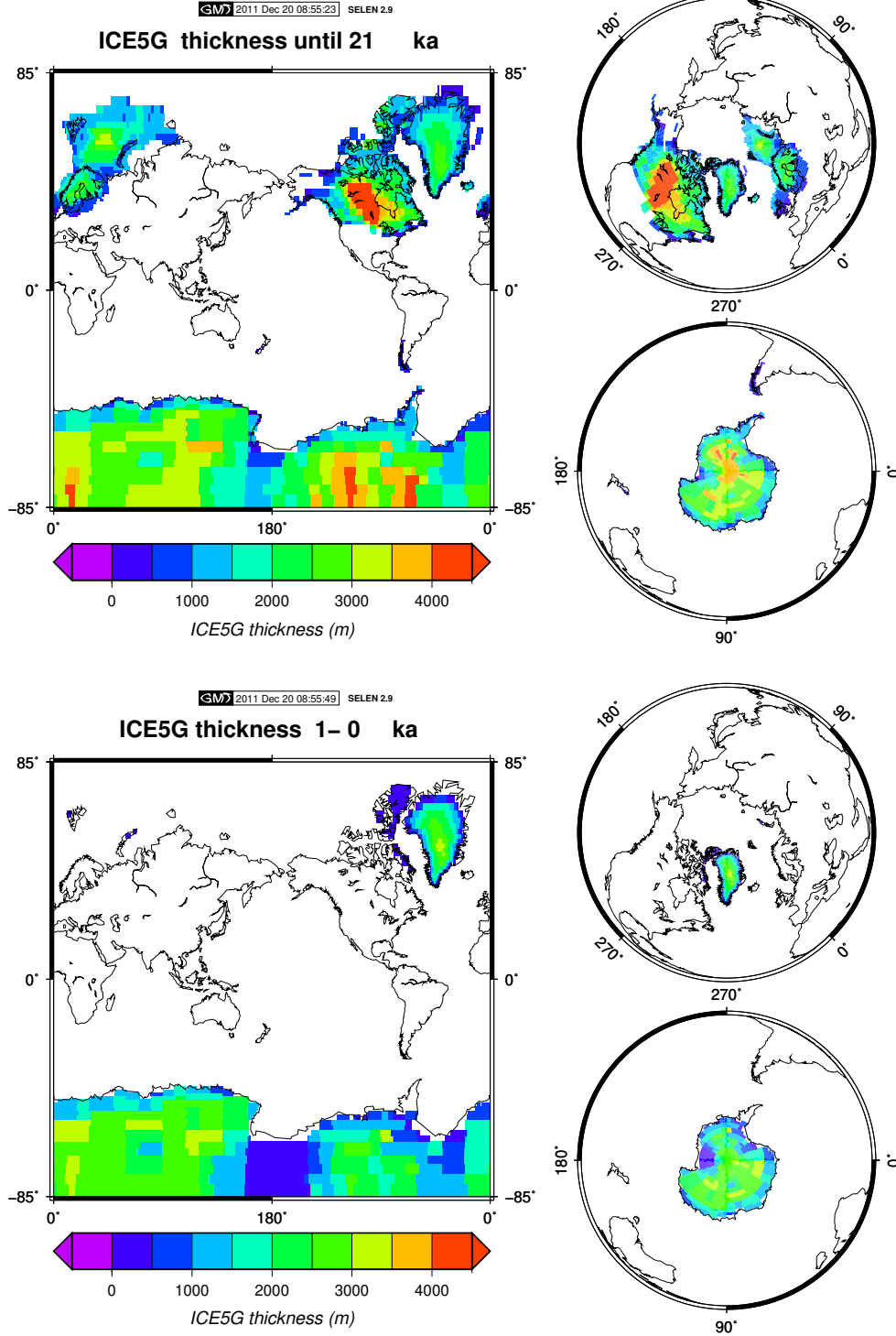


Figure 4: Ice thickness $T(\omega, t)$ at the LGM (21 kyrs ago, top) and at during the most recent time increment, between 1 kyr BP and present time (bottom), according to model ICE-5G (Peltier, 2004). The time-history of the Equivalent Sea Level for this model is shown in Fig. 5. Maps for all the other time steps between LGM and present are available in folder `depot-TEST/ICE5G/original`.

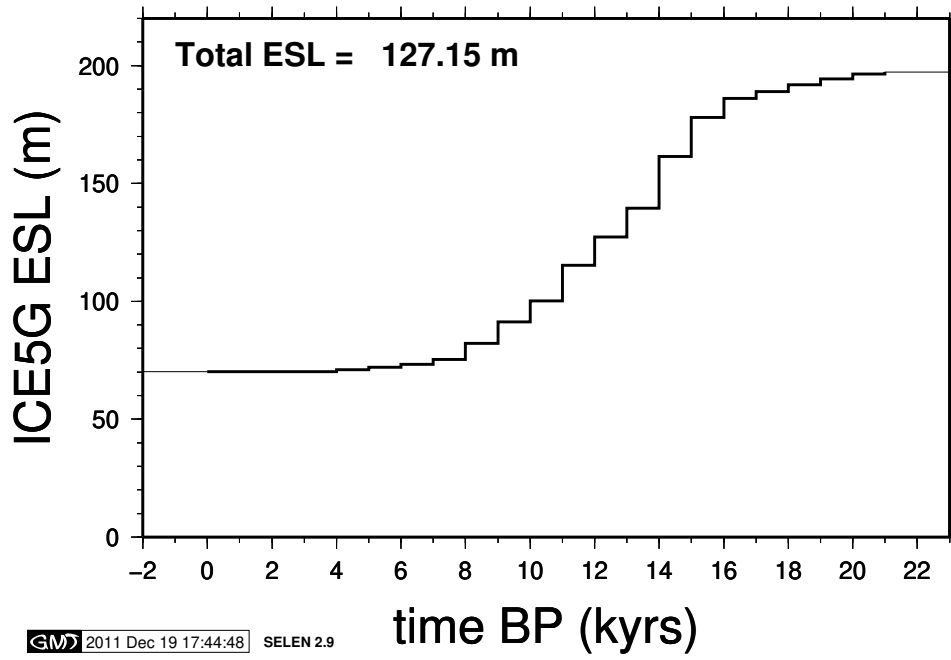


Figure 5: Equivalent Sea Level for model ICE-5G (Peltier, 2004). At a given time t before present, $ESL(t) = (\rho_i/\rho_w)(V_i(t) - V_i(t_p))/A_o$, where $V_i(t)$ is the ice volume, $V_i(t_p)$ is present day volume, and A_o is the area of the oceans surface. Hence, according to Eq. (10), the plot of ESL mirrors that of S^E . The total ESL variation (~ 127 m) represents the difference between ESL at the LGM and the present day value.

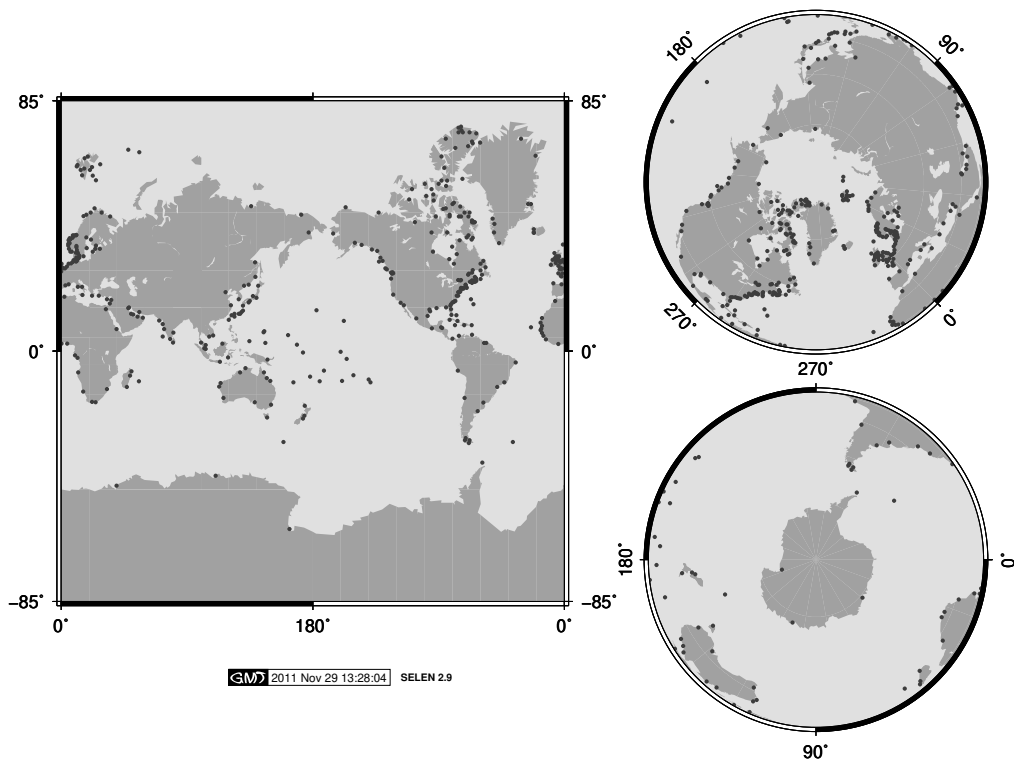
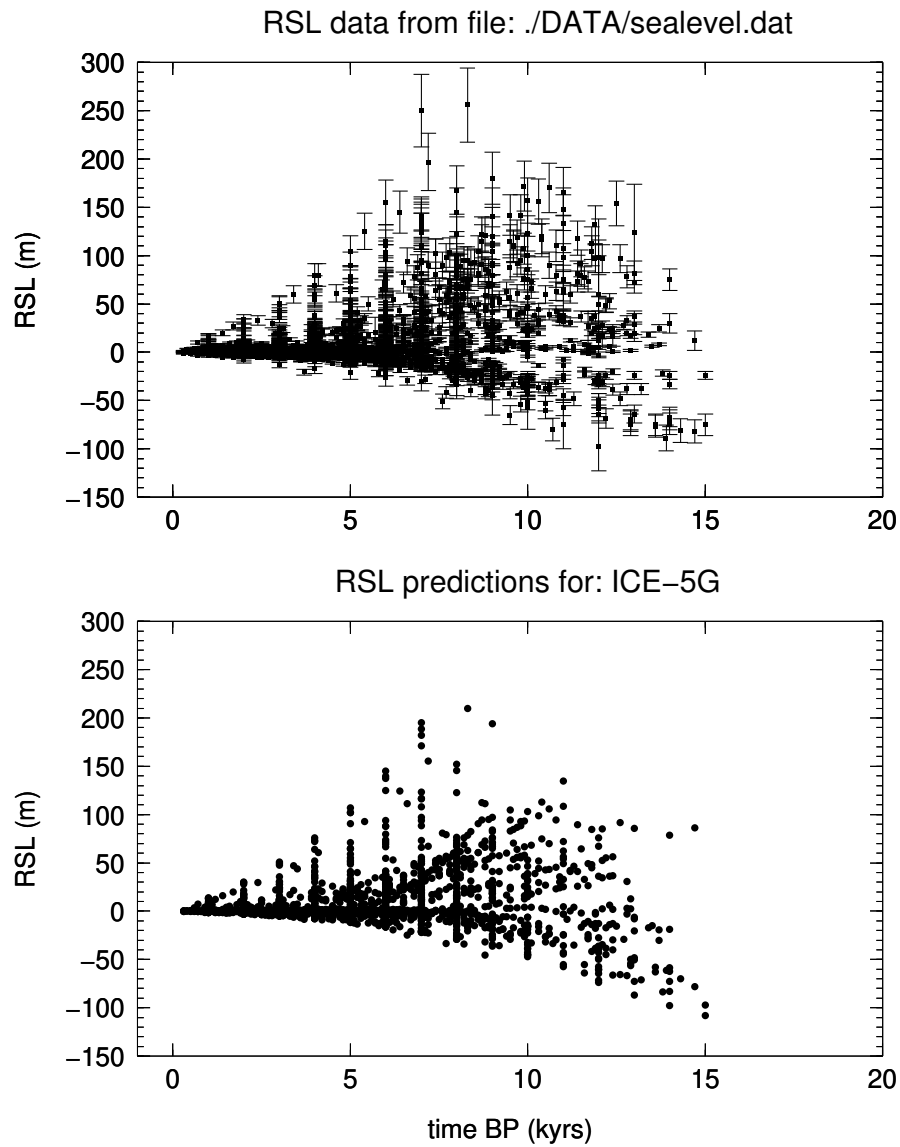


Figure 6: Geographical distribution of the 392 sites in file `sealevel.dat`, from which information about the history of RSL during the last $\sim 15,000$ years is available. This plot and more data about these sites are available from `depot-TEST/rs1/rs1-sites`.




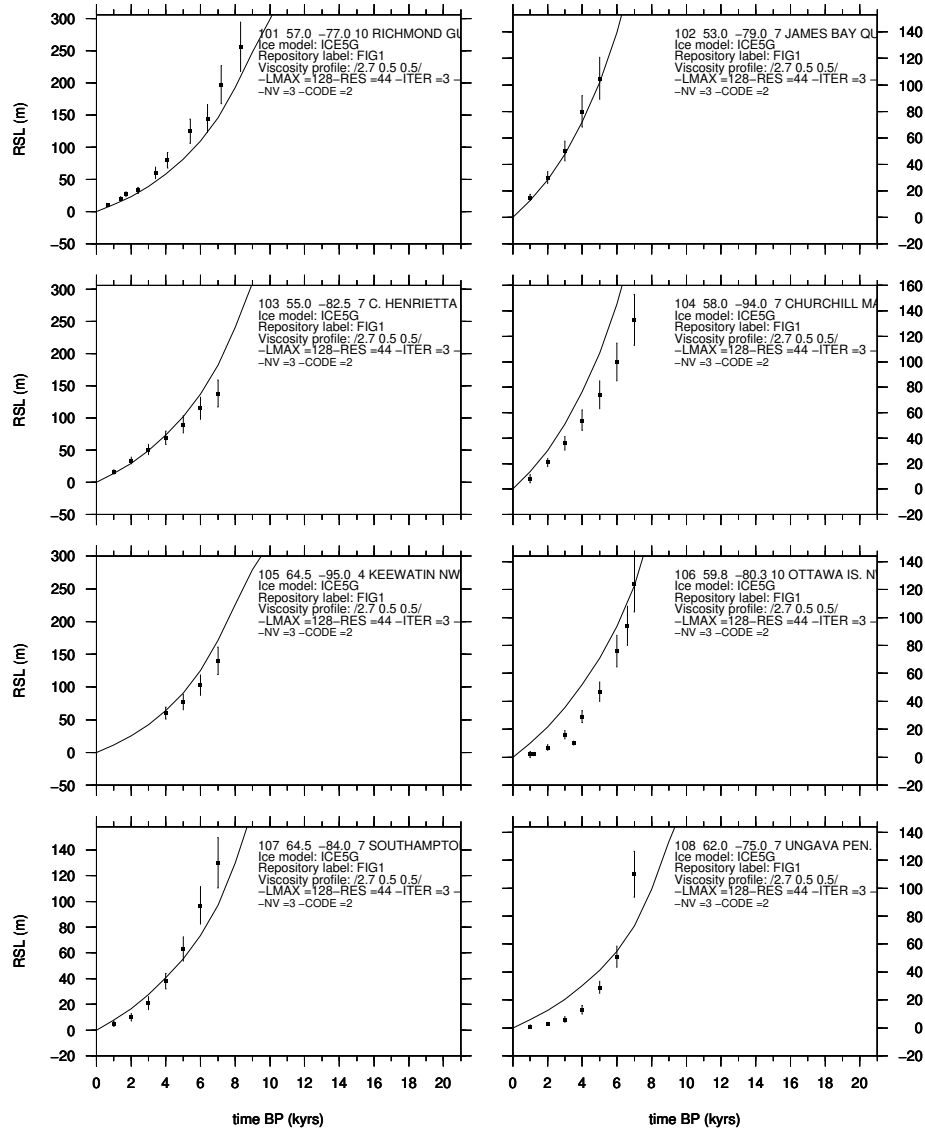
 2011 Nov 29 13:18:17 SELEN 3.2

Figure 7: Scatterplot showing RSL observations (top) from sites of the compilation of Tushingham and Peltier (1992, 1993). RSL predictions, obtained solving the SLE in our TEST run of SELEN, are shown in the bottom frame.



GM 2011 Dec 23 17:32:54 SELEN 2.9

Figure 8: RSL observations (with error bars) pertaining to the eight sites of Hudson bay in file `sealevel.dat`, compared with SELEN predictions (solid curves). Basic parameters for the TEST run are summarized in each frame. Postscript and PDF figures are located `depot-TEST/rsl/rsl-curves/ps` and `depot-TEST/rsl/rsl-curves/pdf`, respectively.

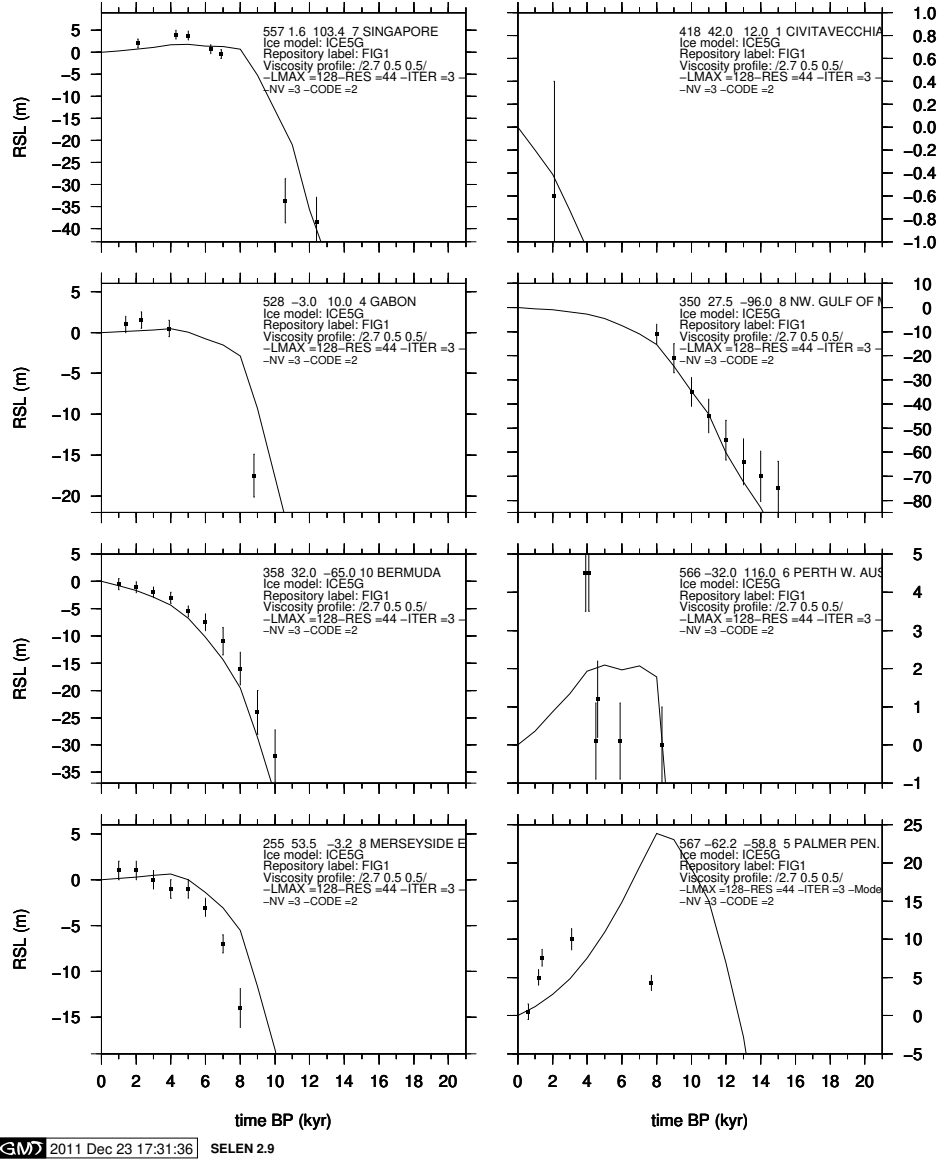


Figure 9: RSL curves at eight miscellaneous sites located in the far field of the former ice sheets: Singapore, Civitavecchia (Italy), Gabon, NW Gulf of Mexico, Bermuda, Perth W. Australia, Merseyside (England), and Palmer peninsula (Antarctica). All the RSL predictions for the TEST run are found in `depot-TEST/rsl/rsl-curves`.

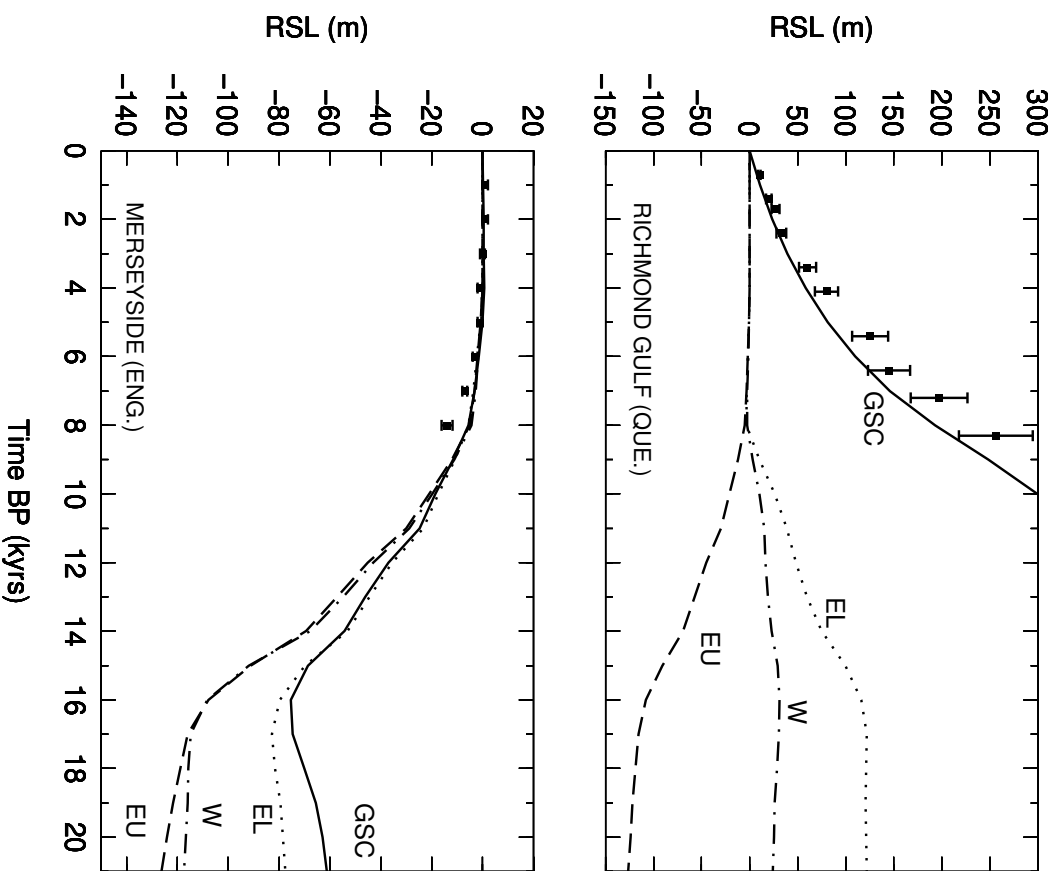


Figure 10: Comparison of the outcomes of various SELÉN runs, in which the SLE is solved using various approximations (GSC: gravitationally self-consistent, EL: elastic, W: Woodward, EU: Eustatic). Top and bottom frames show results for Richmond Gulf (Hudson bay) and Merseyside (England), respectively.

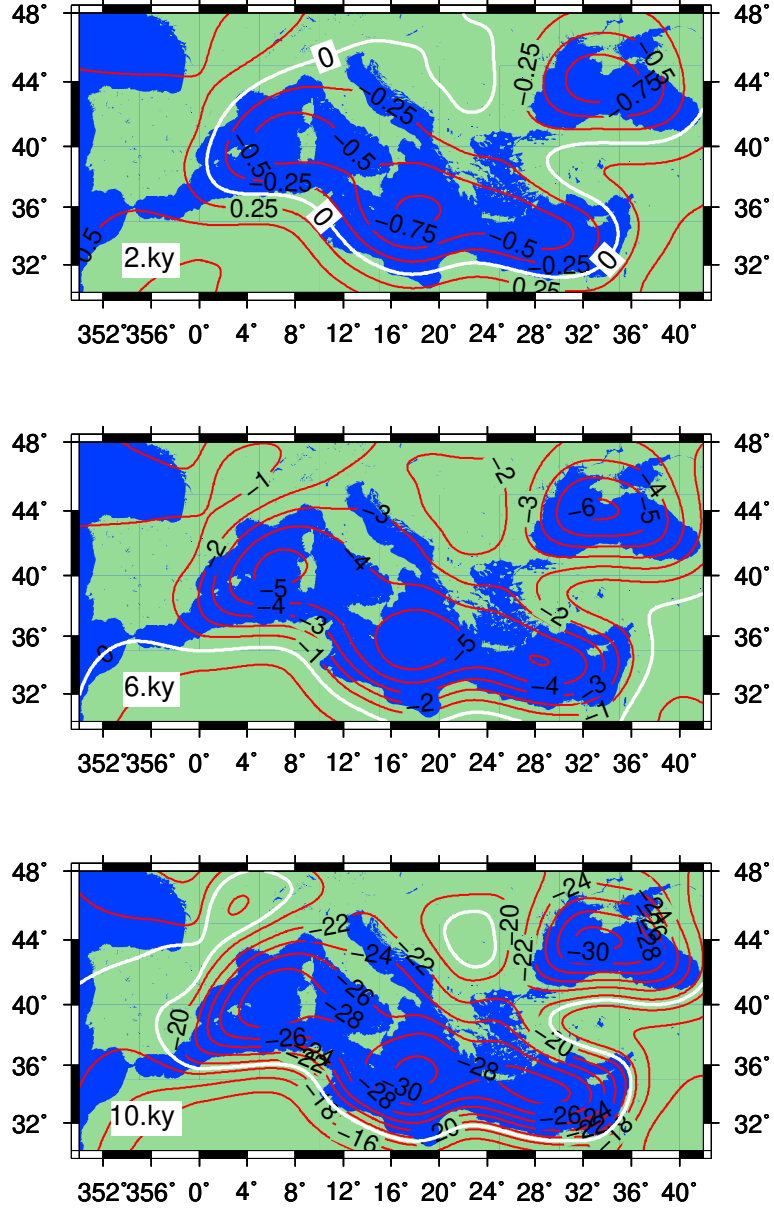
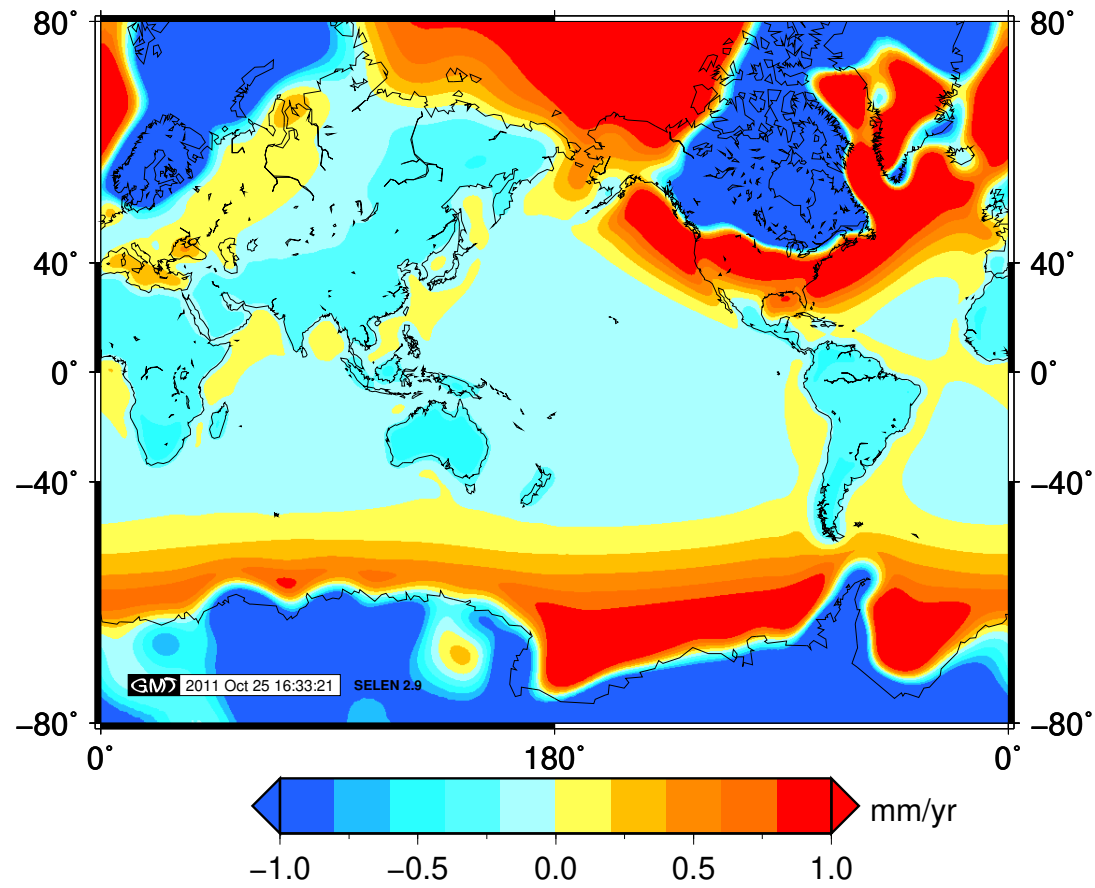


Figure 11: Example of RSL contour plot for the Mediterranean region, at times 2, 6, and 10 kyrs BP. These correspond to three different configurations of file `DATA/rs1-region.dat`, all based on the SELEN parameters employed in the TEST run (ice model ICE-5G and rheological parameters in Table 5).

Rate of sea level change today

–Ice model: ICE5G –Viscosity profile: /2.7 0.5 0.5/



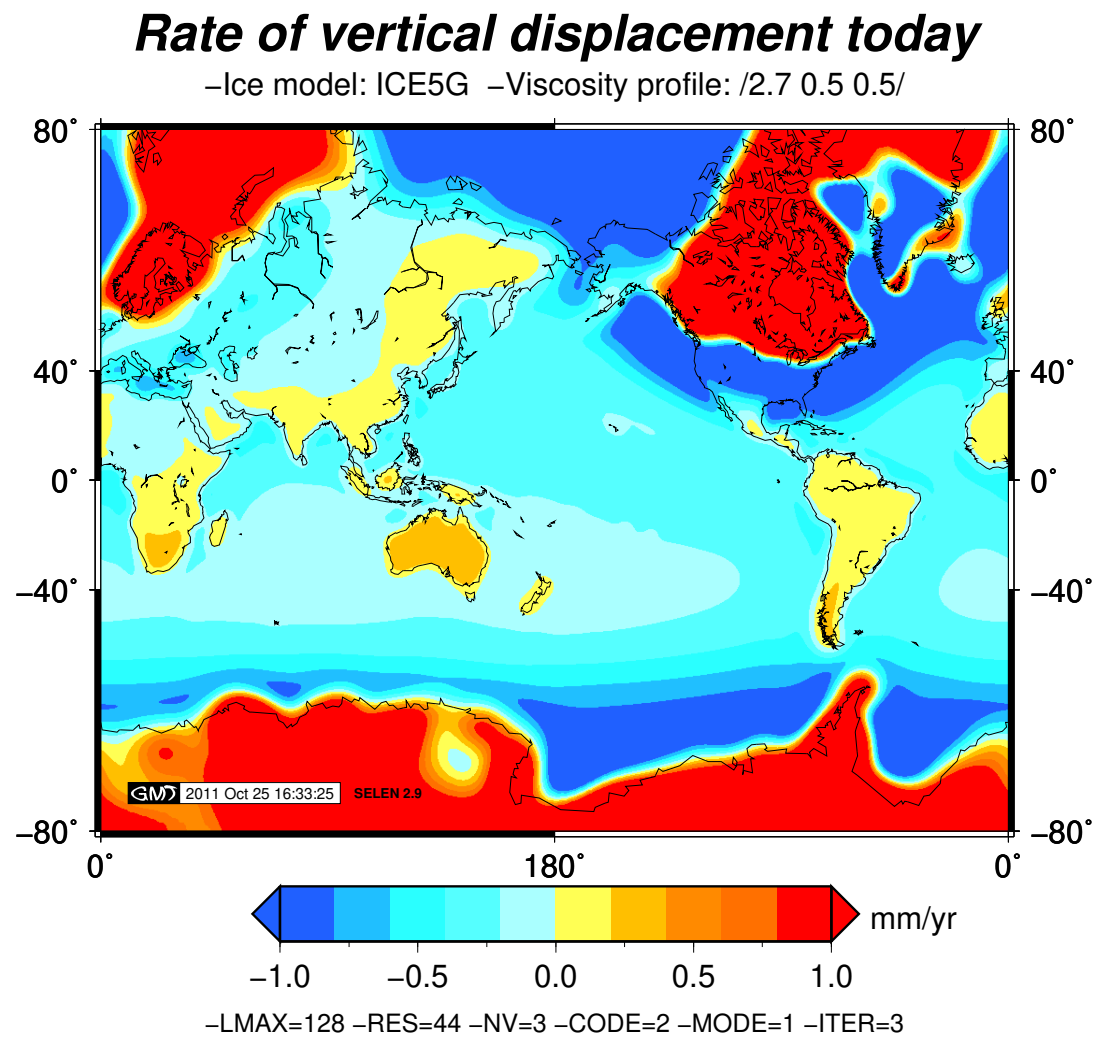


Figure 13: Global map of GIA-induced vertical velocity (\dot{S}) for our TEST run. Subsiding and uplifting areas are shown by blue and red hues, respectively. In this map, the \dot{U} values vary in the range $[-3.5/19.2]$ mm/yr.

Rate of geoid height variation today

–Ice model: ICE5G –Viscosity profile: /2.7 0.5 0.5/

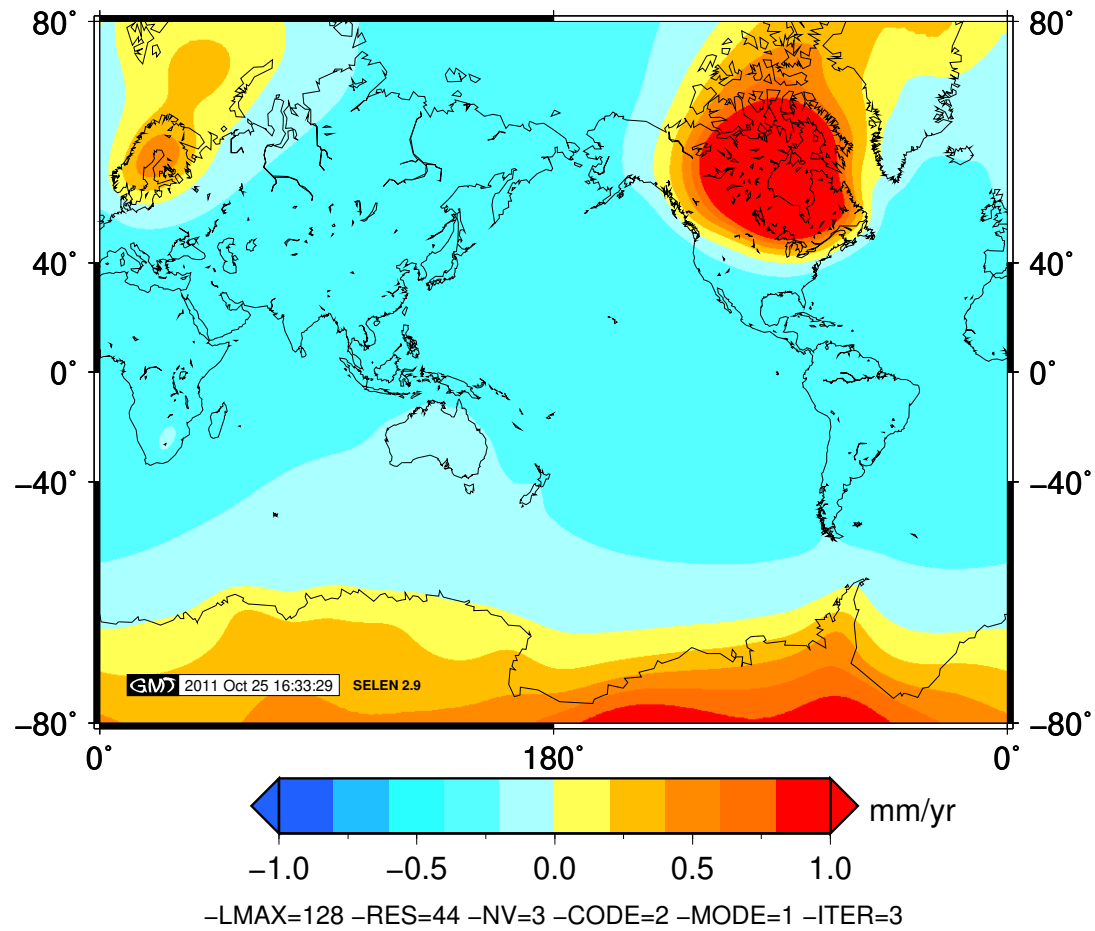


Figure 14: Global map showing the sea surface variation induced by GIA, relative to the Earth's center of mass (\dot{N}), for run TEST. The range of variation of \dot{N} on this map is $[-0.4/2.3]$ mm/yr.

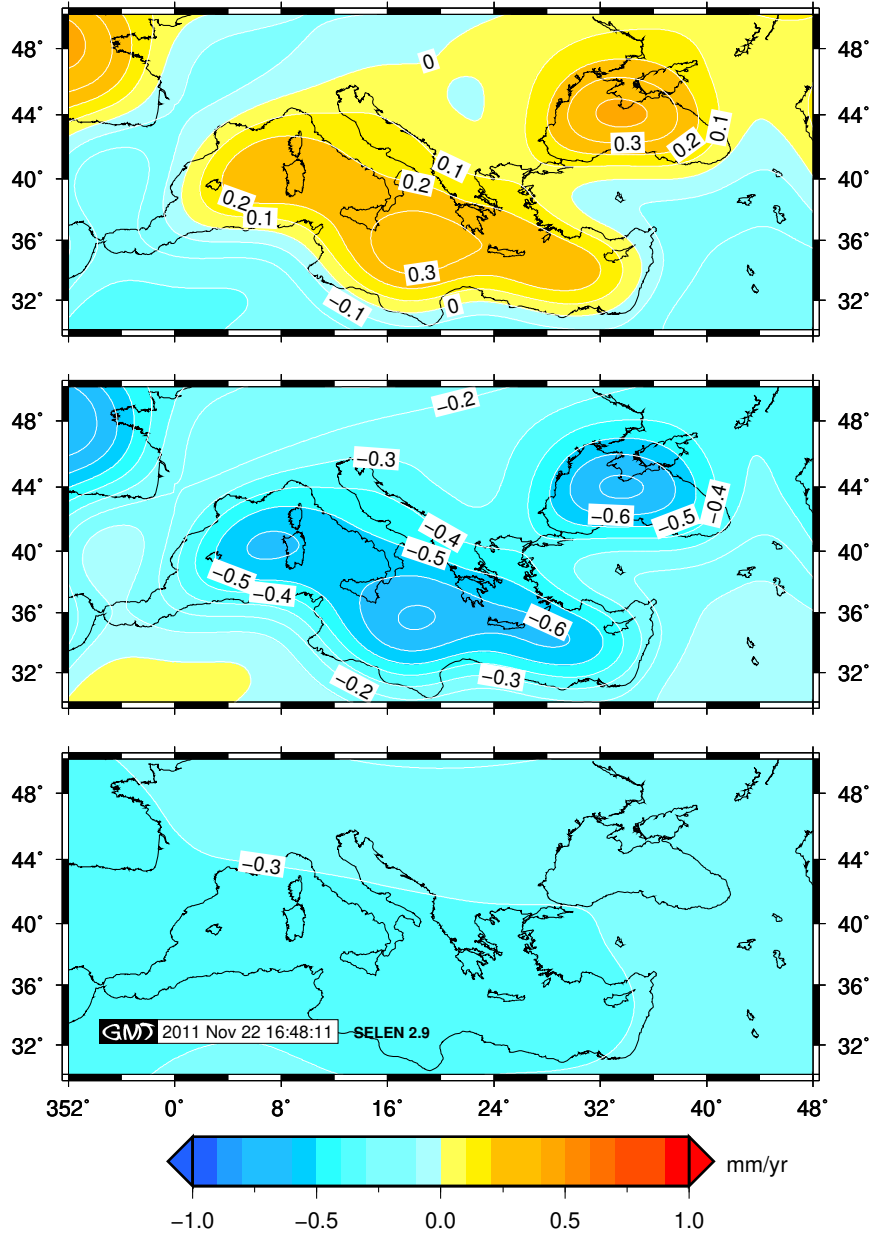
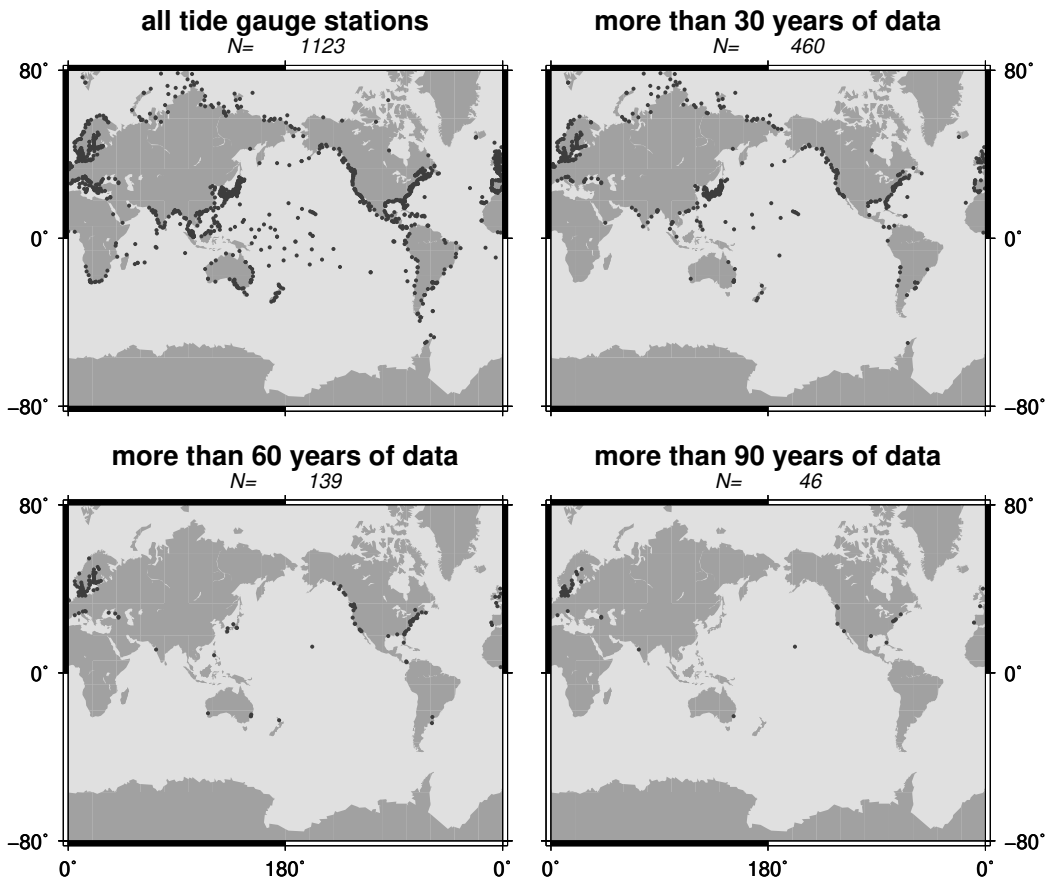


Figure 15: Regional analysis showing rates of sea level change (\dot{S} , top), of vertical uplift (\dot{U} , middle) and sea surface variation (\dot{N} , bottom) across the Mediterranean region, for run TEST. Data and plots for this analysis are found in folder depot-TEST/rmaps.



GM 2011 Nov 29 10:40:56 SELEN 2.9

Figure 16: Geographical distribution of the TGs considered in run TEST, according to the number of RLR data available from each station. Data and plots for this analysis are available in `depot-TEST/tgauges/ tgauges-sites` after the execution of SELEN.

Station Name	valid yearly records	time range year-year	trend r_k mm/yr	error σ_k	r_k^{gta} mm/yr	N mm/yr	\bar{U} mm/yr
Kungholmsfort	118	1887–2005	−0.04	0.13	−1.48	+0.03	+1.52
Olands Norra Udde	119	1887–2005	−1.14	0.14	−2.60	+0.13	+2.76
Landsort	119	1887–2005	−2.91	0.14	−4.18	+0.23	+4.44
Nedre Sodertaje	102	1869–1970	−3.44	0.19	−4.73	+0.27	+5.02
Stockholm	117	1889–2005	−3.90	0.15	−4.89	+0.28	+5.20
Ratan	112	1892–2005	−7.81	0.18	−8.95	+0.53	+4.49
Helsinki	124	1879–2004	−2.43	0.16	−4.23	+0.29	+4.55
Swinoujscie	180	1811–1999	+0.82	0.06	−0.43	−0.08	+0.35
Warnemunde 2	149	1856–2005	+1.20	0.07	−0.36	−0.09	+0.27
Wismar 2	156	1849–2005	+1.39	0.06	−0.26	−0.11	+0.15
Kobenhavn	104	1889–2002	+0.39	0.11	−0.99	−0.02	+0.98
Fredericia	105	1890–2002	+1.01	0.08	−0.57	−0.06	+0.52
Aarhus	101	1889–2002	+0.55	0.08	−0.95	−0.03	+0.93
Esbjerg	103	1890–2002	+1.18	0.14	−0.35	−0.08	+0.27
Cuxhaven 2	160	1843–2002	+2.44	0.09	−0.01	−0.14	−0.12
Aberdeen II	103	1862–1965	+0.58	0.10	−0.43	−0.17	+0.28
Marseille	108	1886–2004	+1.28	0.08	+0.08	−0.30	−0.39
Poti	121	1874–2004	+6.55	0.15	+0.03	−0.28	−0.31
Batumi	106	1882–2005	+1.78	0.20	+0.00	−0.28	−0.29
Mumbai/Bombay	111	1878–1993	+0.78	0.09	−0.17	−0.27	−0.10
Sydney, F. Denison	108	1886–1993	+0.59	0.09	−0.32	−0.16	+0.15
Honolulu	101	1905–2005	+1.48	0.12	−0.16	−0.35	−0.18
Seattle	106	1899–2005	+2.06	0.10	+0.71	−0.02	−0.73
San Francisco	151	1855–2005	+1.43	0.08	+0.68	−0.32	−0.99
Baltimore	102	1903–2005	+3.11	0.10	+1.15	−0.10	−1.25
New York	131	1856–2005	+2.76	0.06	+1.13	−0.05	−1.19

Table 4: Present-day trends of GIA-induced sea level change, sea surface variation, and vertical velocity at RLR PSMSL TGs with more than 100 valid years in the record series. With r_k and σ_k we denote the best-fit secular rates and their uncertainties. This is an excerpt of the ASCII table `depot-TEST/ tauges/ tgauges-predictions/ ptidegauges`.

Station Name	valid yearly records	time range year–year	trend r_k mm/yr	error σ_k	r_k^{gia} mm/yr	\dot{N} mm/yr	\dot{U} mm/yr
Algeciras	34	1944–2001	+0.46	0.25	−0.21	−0.33	−0.11
Tarifa	46	1944–2001	+0.02	0.39	−0.21	−0.33	−0.12
Malaga	41	1994–2001	+2.41	0.43	−0.23	−0.32	−0.09
Alicante II	30	1960–1995	−0.85	0.27	−0.07	−0.32	−0.25
Marseille	108	1886–2004	+1.28	0.08	+0.08	−0.30	−0.39
Genova	78	1884–1992	+1.20	0.07	+0.07	−0.29	−0.36
Venezia (S. Stefano)	45	1872–1919	+2.55	0.42	+0.04	−0.27	−0.31
Venezia (P. Salute)	82	1909–2000	+2.39	0.16	+0.04	−0.27	−0.31
Trieste	96	1905–2006	+1.17	0.12	+0.04	−0.27	−0.31
Rovinj	48	1956–2004	+0.53	0.29	+0.06	−0.27	−0.34
Bakar	62	1930–2004	+0.97	0.23	+0.05	−0.27	−0.32
Split Rt Marjana	50	1953–2004	+0.60	0.30	+0.10	−0.30	−0.39
Split Harbour	50	1955–2004	+0.33	0.30	+0.10	−0.29	−0.39
Ceuta	51	1945–2005	+0.38	0.23	−0.21	−0.33	−0.11

Table 5: Present–day trends of GIA–induced sea level change, sea surface variation, and vertical velocity at RLR Mediterranean PSMSL TGs with more than 30 valid years in the record series.

–Ice model: ICE5G –Viscosity profile: /2.7 0.5 0.5/ –LMAX=128 –RES=44 –NV=3 –CODE=2 –MODE=1 –ITER=3

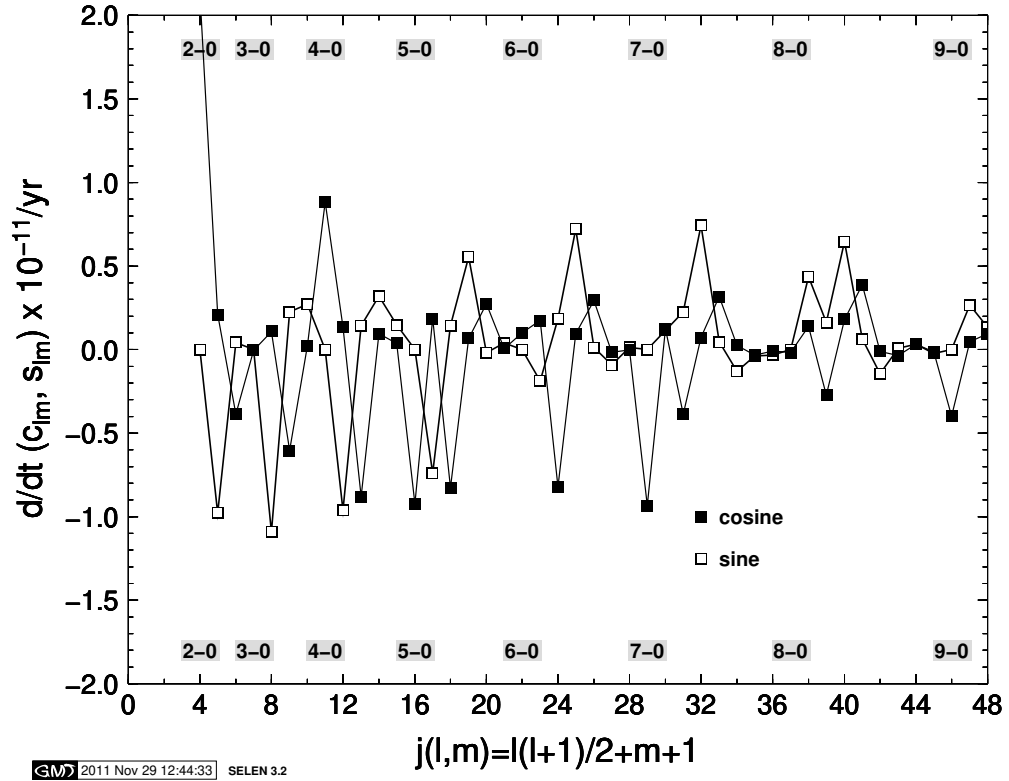


Figure 17: Time-derivatives of the Stokes coefficients of the Earth’s gravity field associated with GIA, as a function of the generalized harmonic degree $j = \ell(\ell + 1)/2 + m + 1$ for $2 \leq \ell \leq 9$ and $0 \leq m \leq \ell$. Output data for this analysis are found in folder `depot-TEST/stokes` after the execution of SELEN.

References

- Cianetti S, Giunchi C, Spada G (2002) Mantle viscosity beneath the Hudson Bay: an inversion based on the Metropolis algorithm. *J. Geophys. Res.* 107(B12):2352. doi:10.1029/2001JB000585
- Clark JA, Farrell WE, Peltier WR (1978) Global changes in postglacial sea level: a numerical calculation. *Quat. Res.* 9:265–287.
- Douglas BC (1997) Global sea-level rise: a redetermination. *Surv. Geophys.* 18:279–292.
- Ewert H, Groh A, Dietrich R (2012) Volume and mass changes of the Greenland ice sheet inferred from ICESat and GRACE. *Journal of Geodynamics* 59-60:111-123. doi: 10.1016/j.jog.2011.06.003
- Farrell WE, Clark JA (1976) On postglacial sea-level. *Geophys. J. R. Astron. Soc.* 46:647–667.
- Fenoglio-Marc L, Rietbroek R, Grayek S, Becker M, Kusche J, Stanev E (2012) Water mass variation in the Mediterranean and Black Seas. *Journal of Geodynamics* 59–60:168–182.
- Groh A, Ewert H, Scheinert M, Fritsche M, Rülke A, Richter A, Rosenau R, Dietrich R (2012) An investigation of Glacial Isostatic Adjustment over the Amundsen Sea sector, West Antarctica. *Global and Planetary Change* 98–99:45–53. 10.1016/j.gloplacha.2012.08.001
- King MA, Altamimi Z, Boehm J, Bos M, Dach R, Elosegui P, Fund F, Hernández-Pajares M, Lavalée D, Mendes Cerveira PJ, Penna N, Riva REM, Steigenberger P, Van Dam T, Vittuari L, Williams S, Willis P (2012) Improved constraints on models of Glacial Isostatic Adjustment: a review of the contribution of ground-based geodetic observations. *Surv. Geophys.* 31:465–507. doi:10.1007/s10712-010-9100-4
- Lambeck K, Chappell J (2001) Sea Level Change Through the Last Glacial Cycle. *Science* 292:679–686.
- Lambeck K, Antonioli F, Purcell A, Silenzi S (2004) Sea-level change along the Italian coast from the past 10,000 years. *Quat. Sci. Rev.* 23:1567–1598.
- Lambeck K, Purcell A (2005) Sea-level change in the Mediterranean Sea since the LGM: model predictions for tectonically stable areas. *Quat. Sci. Rev.* 24:1969–1988.
- Milne GA, Mitrovica JX (1998) Postglacial sea-level change on a rotating Earth. *Geophys. J. Int.* 133:1–10.
- Mitrovica JX, Peltier WR (1991) On post-glacial geoid subsidence over the equatorial ocean. *J. Geophys. Res.* 96:20,053–20,071.
- Mitrovica JX, Davis JL, Shapiro II (1994) A spectral formalism for computing three-dimensional deformations due to surface loads. *J. Geophys. Res.* 99:7057–7073.
- Mitrovica JX, Peltier WR (1992) Constraints on mantle viscosity from relative sealevel variations in Hudson Bay. *Geophys. Res. Lett.* 19:1185–1188.
- Mitrovica JX, Tamisiea ME, Davis JL, Milne GA (2001) Recent mass balance of polar ice sheets inferred from patterns of global sea-level change, *Nature* 409:1026–1029.
- Mitrovica JX, Milne GA (2002) On the origin of Late-Holocene highstands within equatorial ocean basins. *Quat. Sci. Rev.* 21:2179–2190.
- Nielsen K, Khan SA, Korsgaard NJ, KH Kjær, Wahr J, Bevis M, Stearns LA, Timm LH (2012) Crustal uplift due to ice mass variability on Upernavik Isstrøm, west Greenland. *Earth and Planetary Science Letters* 353–354:182–189. doi:10.1016/j.epsl.2012.08.024

- OpenMP (2005) OpenMP Application Program Interface, Version 2.5. OpenMP Architecture Review Board, <http://www.openmp.org/mpdocuments/spec25.pdf> (last accessed 2011).
- Peltier WR (1974) The impulse response of a Maxwell earth. *Rev. Geophys. Space Phys.* 12:649–669.
- Peltier WR (2001) Global glacial isostatic adjustment and modern instrumental records of relative sea level history. In: *Sea Level Rise: History and Consequences*. Academic Press, San Diego, pp. 65–95.
- Peltier WR (2004) Global glacial isostasy and the surface of the Ice–Age Earth: the ICE–5G(VM2) model and GRACE. *Annu. Rev. Earth Pl. Sc.* 32:111–149.
- Schubert G, Turcotte D, Olson, P (2004) *Mantle convection in the Earth and Planets*. Cambridge University Press, Cambridge.
- Solomon S, Qin D, Manning M, Chen Z, Marquis M, Averyt KB, Tignor M, Miller HL (2007) *IPCC Climate change 2007: the physical science basis*. Cambridge University Press, Cambridge.
- Sørensen LS (2010) *Changes of the Greenland ice sheet derived from ICESat and GRACE data*. PhD Thesis, University of Copenhagen.
- Sørensen LS, Simonsen SB, Nielsen K, Lucas–Picher P, Spada G, Adalgeirsdottir G, Forsberg R, Hvidberg, CS (2011) Mass balance of the Greenland ice sheet – a study of ICESat data, surface density and firn compaction modelling, *The Cryosphere* 5:173–186. doi:10.5194/tc-5-173-2011
- Spada G (2003) *The theory behind TABOO*. Samizdat Press, Golden, Colorado.
- Spada G, Antonioli A, Boschi L, Cianetti S, Galvani G, Giunchi C, Perniola B, Piana Agostinetti N, Piersanti A, Stocchi P (2004) Modeling Earth’s post–glacial rebound. *Eos. Trans. AGU* 85:62–64.
- Spada G, Stocchi P (2006) *The Sea Level Equation, Theory and Numerical Examples*. Aracne, Roma.
- Spada G, Stocchi P (2007) SELEN: a Fortran 90 program for solving the “Sea Level Equation”, *Comput. and Geosci.* 33(4):538–562. doi: 10.1016/j.cageo.2006.08.006
- Spada G, Barletta VR, Klemann V, Riva REM, Martinec Z, Gasperini P, Lund B, Wolf D, Vermeersen LLA, King M (2011) A benchmark study for glacial–isostatic adjustment codes. *Geophys. J. Int.* 185:106–132. doi:10.1111/j.1365-246X.2011.04952.x
- Spada G, Ruggieri G, Sorensen LS, Nielsen K, Melini D., Colleoni F (2012) Greenland uplift and regional sea level changes from ICESat observations and GIA modelling, *Geophys. J. Int.* 189:1457–1474. doi: 10.1111/j.1365-246X.2012.05443.x
- Spada G, Galassi G (2012) New estimates of secular sea level rise from tide gauge data and GIA modelling. *Geophys. J. Int.* in press. doi:10.1111/j.1365-246X.2012.05663.x
- Stocchi P, Spada G (2007) Glacio and hydro–isostasy in the Mediterranean Sea: Clark’s zones and role of remote ice sheets. *Ann. Geophys.* 50(6):741–761.
- Stocchi P, Spada G (2009) Influence of glacial isostatic adjustment upon current sea level variations in the Mediterranean. *Tectonophysics* 474:56–68. doi:10.1016/j.tecto.2009.01.003
- Tamisiea ME, Mitrovica JX, Milne GA, Davis JL (2001) Global geoid and sea level changes due to present–day ice mass fluctuations, *J. Geophys. Res.* 106(B12):30,849–30,863. doi:10.1029/2000JB000011

- Tapley B, Bettadpur S, Watkins M, Reigber C (2004) The gravity recovery and climate experiment: Mission overview and early results. *Geophys. Res. Lett.* 31(9):L09607.
- Tegmark M (1996) An icosahedron-based method for pixelizing the celestial sphere. *ApJ Letters* 470:L81–L84.
- Tushingham AM, Peltier WR (1991) ICE-3G - A New Global Model of Late Pleistocene Deglaciation Based Upon Geophysical Predictions of Post-Glacial Relative Sea Level Change. *J. Geophys. Res.* 96:4497–4523.
- Tushingham AM, Peltier WR (1992) Validation of the ICE-3G model of Würm-Winsconsin deglaciation using a global data base of relative sealevel histories. *J. Geophys. Res.* 97:3285–3304.
- Tushingham AM, Peltier WR (1993) Relative Sea Level Database. IGPB PAGES/World Data Center-A for Paleoclimatology Data Contribution Series # 93-106. NOAA/NGDC Paleoclimatology Program, Boulder, USA.
- Wessel P, Smith WHF (1998) New, improved version of generic mapping tools released. *Eos. Trans. AGU* 79:579.
- Wu P, Peltier WR (1983) Glacial isostatic adjustment and the free-air gravity anomaly as a constraint on deep mantle viscosity. *Geophys. J. R. Astron. Soc.* 74:377–449.